

The sensitivity of simulated surface-level pollution concentrations to WRF-ARW-model PBL parameterisation schemes over the Highveld of South Africa

Anzel de Lange^{*, a}, Mogesh Naidoo^b, Rebecca M. Garland^{a, b}, Liesl L. Dyson^a

^a *Department of Geography, Geoinformatics and Meteorology, University of Pretoria (UP), Hatfield, 0028, South Africa*

^b *Council for Scientific and Industrial Research (CSIR), Climate and Air Quality Modelling Research Group, Pretoria, 0001, South Africa*

*Corresponding author

Email: anzel.delange@up.ac.za

Tel.: +27 82 779 8493

Abstract

An understanding of the sensitivity of pollutant concentrations to planetary boundary layer (PBL) schemes in numerical weather prediction (NWP) models can provide insight into model results, and possibly advance the accuracy of air pollution modelling. Meteorological output from the Advanced Research Weather Research and Forecasting (WRF-ARW) model, with four frequently used PBL schemes, is used as input for an air quality model. The simulations resulting from the different schemes are compared with each other and evaluated making use of observational air pollution concentration data for a spring and a winter month of 2016 in South Africa. Sensitivity exists in surface-level pollution concentrations as simulated by the considered PBL schemes. No single PBL scheme consistently performed best across the five considered pollutants, five sites and two seasons. During analysis of the air quality simulations, it was found that the two local closure schemes – Mellor-Yamada-Janjić (MYJ) and Mellor-Yamada Nakanishi Niino (MYNN) – often performed well, while the non-local closure schemes – Yonsei University (YSU) and Asymmetric Convection Modelling (ACM) – featured as best-performing schemes the least number of times. Sensitivity also exists on a spatial scale between schemes when simulating sulphur dioxide (SO₂) plumes from tall stacks, and the MYNN scheme frequently produced the highest concentrations of SO₂. The results from this study should be considered when configuring NWP models for the simulation of air quality in the Highveld region.

Keywords: South Africa, WRF model, PBL schemes, air quality modelling, model evaluation

1. Introduction

The circumstances for conducting air quality research in certain countries are challenging due to a lack of good-quality, high spatial resolution pollutant concentration and emission data. However, a comprehensive understanding of an air quality situation is nevertheless needed to combat air pollution problems. A means whereby the above-mentioned data issues can be partially addressed is by using models for the simulation of meteorological variables, as well as air quality. A very valued instrument in this field of atmospheric research is the NWP model. Meteorological and air quality models have been used for decades in air quality-related studies (Ritter *et al.*, 2013). Models are a cost-effective way of producing high-resolution simulations of ambient pollution concentrations. These models are well positioned to assist countries without large monitoring networks to better understand their local air pollution problems. The representativeness of air quality model simulations is dependent on the model parameterisation chosen during setup, the accuracy of the meteorological input, the completeness of the emissions data, and geophysical data (DEA, 2013).

Therefore, the subject of air quality modelling is an important one, particularly in countries with serious air pollution problems. South Africa has three declared air pollution priority areas where national ambient air quality standards are being exceeded or are expected to be exceeded, and where focused air quality management action is needed. The Highveld Priority Area (HPA) and the Vaal Triangle Airshed Priority Area (VTAPA) were declared due to poor air quality caused primarily by industrial emitters, emissions from large urban areas, domestic fuel and waste burning, and vehicular sources (DEAT, 2006; DEAT, 2007). The Waterberg-Bojanala Priority Area (WBPA), located in the North West and Limpopo provinces (Figure 1), was proactively declared due to planned development that was expected to dramatically decrease air quality in the area (DEA, 2012). Pollutant concentration levels in South Africa often exceed South African National Ambient Air Quality Standards (NAAQS), as well as the recommendations of the World Health Organisation (WHO), where measurements are available (e.g. Belelie *et al.*, 2019; Cairncross *et al.*, 2018).

While an accurate emission inventory plays a significant role in ensuring accurate simulations of pollutant concentrations, the setup of the preceding meteorological model is also of utmost importance. Air quality models use the prognostic fields from NWP models as input; therefore, the successful simulation of air quality also depends heavily on the accuracy of these inputs (Rogers *et al.*, 2013).

The use of air quality models has the advantage of greater spatial coverage (in comparison to air quality measurements), but any errors in the simulation of meteorological fields will be passed on to the air quality model and will have an effect on its outputs. Therefore, the accurate simulation of meteorological parameters, which are known to have an influence on the pollution dispersion and chemistry of the atmosphere, is of utmost importance (Gilliam *et al.*, 2006).

Most NWP models contain multiple physics options for parameterisations, such as PBL, surface layer, microphysics, cumulus parameterisation, longwave radiation and shortwave radiation schemes, among others. In order to optimally set up the model for a specific region, these options need to be investigated, and the most appropriate parameterisation schemes chosen. Effort should be made to use the most appropriate options when configuring PBL schemes in meteorological modelling and chemical transport pre-processors, while performing air quality simulations (Pérez *et al.*, 2006). This is crucial, not only because meteorology affects the dispersion and transportation of pollutants in the atmosphere, but also its effects on chemical transformation and removal (Ocak and Turalioglu, 2008). Chemical processes in the atmosphere are dependent on temperature, radiation and relative humidity, and the dependencies are highly complex (Radaideh, 2017; Kong *et al.*, 2015).

The choice of a PBL scheme in an NWP model affects simulated PBL height, as well as other meteorological parameters, like temperature, humidity, wind speed and direction (De Lange *et al.*, 2021), which, in turn, influence the simulated concentrations of air pollution. A substantial amount of research has gone into the sensitivity testing of different PBL and other schemes, and their influence on outputs from air quality models (Banks and Baldasano, 2016; Cuchiara *et al.*, 2014; Kim *et al.*, 2015; Liao *et al.*, 2014; Pérez *et al.*, 2006; Tao *et al.*, 2013; Wang *et al.*, 2019). However, none exist for South Africa.

In studies of this type, it would be desirable to identify a single best-performing PBL scheme for all pollutants investigated within a region, but this may not be a realistic expectation. For instance, using the WRF-ARW model, Banks and Baldasano (2016) found inconsistency in the performance of simulated pollutant concentration results as one scheme could not be identified as being the best-performing scheme across all the considered pollutants. The ACM scheme produced the lowest bias with respect to ozone (O_3), while the YSU scheme performed best with simulated nitrogen dioxide (NO_2). When considering a single pollutant case study, a best-performing scheme might be identifiable, as in Cuchiara *et al.* (2014), where four

different PBL schemes were considered when simulating O₃ concentrations over Houston. It was found that the YSU scheme showed the greatest agreement with observed values.

The effect of different NWP model configurations on air quality in South Africa has not yet been investigated, but some research has been conducted on the topic of NWP model configurations and their effect on meteorological parameters. The simulation of rainfall using the WRF-ARW model with different parameterisations for atmospheric convection has been studied in South Africa (Crétat *et al.*, 2012; Pohl *et al.*, 2014; Ratna *et al.*, 2014). Crétat *et al.* (2012) identified a suitable configuration of the WRF-ARW model for the regional climate of southern Africa with respect to rainfall. The sensitivity of simulated wind speed to different physics options in the WRF-ARW model was also investigated when producing the Wind Speed Atlas for South Africa (WASA) (Hahmann *et al.*, 2015). In addition, De Lange *et al.* (2021) considered different WRF-ARW-model PBL configurations to establish a preferred scheme for use when simulating different meteorological variables for the Highveld region.

The heavily polluted Highveld region (Figure 1; Grid 2) forms the domain under investigation in this study and includes the HPA and the VTAPA. The Highveld region of South Africa is notable for being an air pollution hotspot, hence the declaration of the HPA. The air pollution problem in this area can be partly attributed to the frequently occurring stable meteorological conditions. These conditions are especially dominant during winter and are not conducive to the diffusion and transportation of air pollution (Tyson *et al.*, 1988). The air quality of the area is further impacted on by the large number and diversity of emission sources, which include industry, vehicles, biomass burning, domestic fuel use, waste burning and wind-blown dust. These emission sources contribute to criteria pollutants like nitrogen oxides (NO_x), ozone, particulate matter (PM) and sulphur dioxide in the atmosphere.

The combustion (and incomplete combustion) of fossil fuels, power plants, industrial processes and vehicle emissions all contribute to emissions of NO₂ and SO₂. Another major source of NO₂ and SO₂ emissions in South Africa is domestic fuel combustion, whereby low-income households burn wood, coal or paraffin as a source of heat during winter, and for cooking throughout the year (Hersey *et al.*, 2015). High volumes of private vehicles and traffic on South African roads also contribute significantly to NO₂ and SO₂ emissions (Venter *et al.*, 2012). In addition, NO₂ is formed from the oxidation of nitrogen oxide (NO) in the atmosphere, and a component of NO₂ is produced by natural and biogenic sources (Lazaridis, 2012).

Sources of PM in South Africa are varied and include emissions of primary PM (e.g. fires, unpaved roads and wind-blown dust), as well as many sources of secondary PM (e.g. due to precursor emissions from power plants, domestic fuel combustion, industrial processes, biogenic sources and vehicle emissions). Large-scale biomass burning is a significant contributor to PM pollution (both secondary and primary) and impacts on South Africa from winter into spring (Swap *et al.*, 2003). Domestic fuel combustion is a particularly large source of PM in low-income settlements, and PM concentrations are higher at measurement sites in low-income areas compared to monitoring stations located at industrial and other sites (Hersey *et al.*, 2015). The O₃ concentrations peak during the spring and summer months (September to February) in this area (Balashov *et al.*, 2014), and commonly exceed the South African NAAQS for eight-hour running averages (DEA, 2015)

In this research, a special focus is placed on the simulation of SO₂ concentrations since it is still very relevant in the Highveld due to the abundance of tall stack emissions in the region that impacts on ground-level SO₂ concentrations. Good-quality pollutant concentration data with large spatial coverage is not always available. Therefore, many high-level decisions and reports regarding air quality management are based on model simulations. Models are also useful tools for investigating emission mitigation scenarios. It is therefore vital that simulations of air quality, and specifically the emission of SO₂ from tall stacks, are as accurate as possible in this region.

Tall stack emissions from various industries are considered one of the main contributors to SO₂ pollution in the HPA. On average, power plant stacks in South Africa are approximately 225 m above ground level (AGL) in height. South Africa has 13 coal-fired power plants, with a total generating power of 37 715 Megawatt (MW) (Pretorius, 2015). These are mainly concentrated in the HPA and the VTAPA. Tall stacks, defined as stacks of 500 feet (approximately 150 m) or higher above ground level (US GAO, 2011), are utilised at coal-fired power plants in the study region. While there are many other industries, like petrochemicals and mining operations, concentrated in the HPA and the VTAPA, power stations present some of the tallest stacks (ranging from 150 to 300 m). The tall stacks at these power stations are a dispersion technique that contributes to the dilution of harmful pollutant plumes emitted by power stations (US GAO, 2011). This limits the impact of emissions on local air quality immediately around the station since harmful pollutants are not directly mixed towards the surface near the source. Pollution is instead dispersed, and thus impacts on a larger region, although at much lower concentrations.

When the stacks in the Highveld were designed, a reason for their height was partly due to the need to inject emissions above the height of night-time surface inversions. When these inversions are present, pollutants aloft cannot mix towards the ground as they are emitted above the stable layer. However, after sunrise, when convective conditions prevail, the surface-layer inversion breaks down, allowing pollutants to be transported to the surface level (Collett *et al.*, 2010). The SO₂ emissions from tall stacks are often trapped between inversion layers during the night. During the break-up of these inversion layers, which occurs during the morning, SO₂ is mixed towards the ground. This downward mixing and subsequent peak in SO₂ concentrations usually take place during the morning (between 07:30 and 10:00) in the Highveld region, and coincide with the break-up of the inversion layer (Venter *et al.*, 2012).

Pollutants from power plants, and consequently tall stacks, have been investigated in South Africa (e.g. Belelie *et al.*, 2019; Collett *et al.*, 2010; Venter *et al.*, 2012) because of the environmental and human health threats that these emissions pose. Belelie *et al.* (2019) found that power plants contribute to concentrations of particulate matter with an aerodynamic diameter $\leq 2.5 \mu\text{m}$ (PM_{2.5}), SO₂ and NO₂ in the ambient air of the KwaZamokuhle township, but domestic fuel combustion was identified as the likely major contributor. Collett *et al.* (2010) estimated the total amount of nitrogen deposited in the Highveld region. Tall-stack industrial sources were identified as making a significant contribution to NO_x concentrations at the Elandsfontein ambient air quality monitoring site, which is located in the Highveld region. Venter *et al.* (2012) investigated levels of various pollutants at a site located in the WBPA and found that major sources of SO₂ were high-stack industry emissions, while household combustion from semi-formal and informal settlements was identified as the predominant source of NO₂ and carbon monoxide (CO). The above-mentioned research emphasises the fact that accurate representation of pollutant plumes from power stations is essential, especially in South Africa's priority areas, as many high-level decisions are based on simulations of air pollution. Thus, the accurate representation of the PBL by NWP models is vitally important.

The different configurations of NWP models, together with their effects on the simulation of air quality, have not yet been investigated in South Africa. The main objectives of the presented research are to evaluate the performance and sensitivity of air pollutant concentration simulations in certain PBL schemes contained in the non-hydrostatic WRF-ARW model (Skamarock *et al.*, 2008). Meteorological output from the WRF-ARW model using a range of PBL schemes is used as input to the Comprehensive Air Quality Model with eXtensions (CAMx) (ENVIRON, 2016), together with a locally derived emission inventory for the South African Highveld region.

Model outputs are analysed and compared with measured pollutant concentrations to investigate the general performance of the CAMx model, driven by WRF-ARW output, using different PBL schemes. Additional analysis of simulated SO₂ peak concentrations is undertaken. This research contributes to understanding the sensitivity of the pollutant concentrations of PBL schemes in NWP models, and can provide insight into model results and possibly lead to advances in the accuracy of air pollution modelling in the Highveld region.

2. Study region, experimental setup and model domains

The HPA and the VTAPA encompass the southern and eastern Gauteng, and western Mpumalanga provinces of South Africa (Figure 1). Since pollutant concentration levels are influenced by the rate of emission, as well as meteorological conditions, a winter (June 2016) and a spring (November 2016) case were chosen and used to evaluate the air quality model outputs. Distinctly different meteorological conditions exist in the Highveld region during these months. Choosing different seasons for this study allows the investigation of both the stable and the convective boundary layers. Spring and summer in the region are warm to hot with regular convection (Gijben, 2012), while the continental high dominates in winter, with irregular disruption by mid-latitude systems (Taljaard, 1995). Winters are characterised by very dry and stable atmospheric conditions, and meteorological dispersion potential is considered to be low (Tyson *et al.*, 1988). Pollutants are frequently “trapped” near the surface because of near-surface inversions and low PBL heights (De Lange *et al.*, 2021). In summer and spring, mixing within the PBL is pronounced, and the atmosphere is conditionally unstable (Dyson *et al.*, 2015), resulting in higher PBL heights and favourable pollutant dispersion conditions (De Lange *et al.*, 2019; Lourens *et al.*, 2011).

Table 1. The WRF-ARW model PBL scheme, associated surface-layer schemes and the methods used by the schemes to calculate PBL height (adapted from Banks *et al.*, 2015).

PBL scheme	Surface-layer scheme	PBL height method (<i>threshold</i>)	Reference
Yonsei University (YSU)	MM5 similarity	Richardson Number method (<i>0.00 for unstable and 0.25 for stable PBL</i>)	Hong <i>et al.</i> , 2006
Mellor-Yamada-Janjić (MYJ)	Eta similarity	Total Kinetic Energy (TKE) method (<i>0.2 m²s⁻²</i>)	Janjić, 1994
Mellor-Yamada Nakanishi Niino (MYNN)	MYNN	TKE method (<i>1.0x10⁻⁶ m²s⁻²</i>)	Nakanishi and Niino, 2006
Asymmetric Convection Model 2 (ACM 2)	MM5 similarity	Richardson Number method (<i>0.25 for unstable and stable PBL</i>)	Pleim, 2007

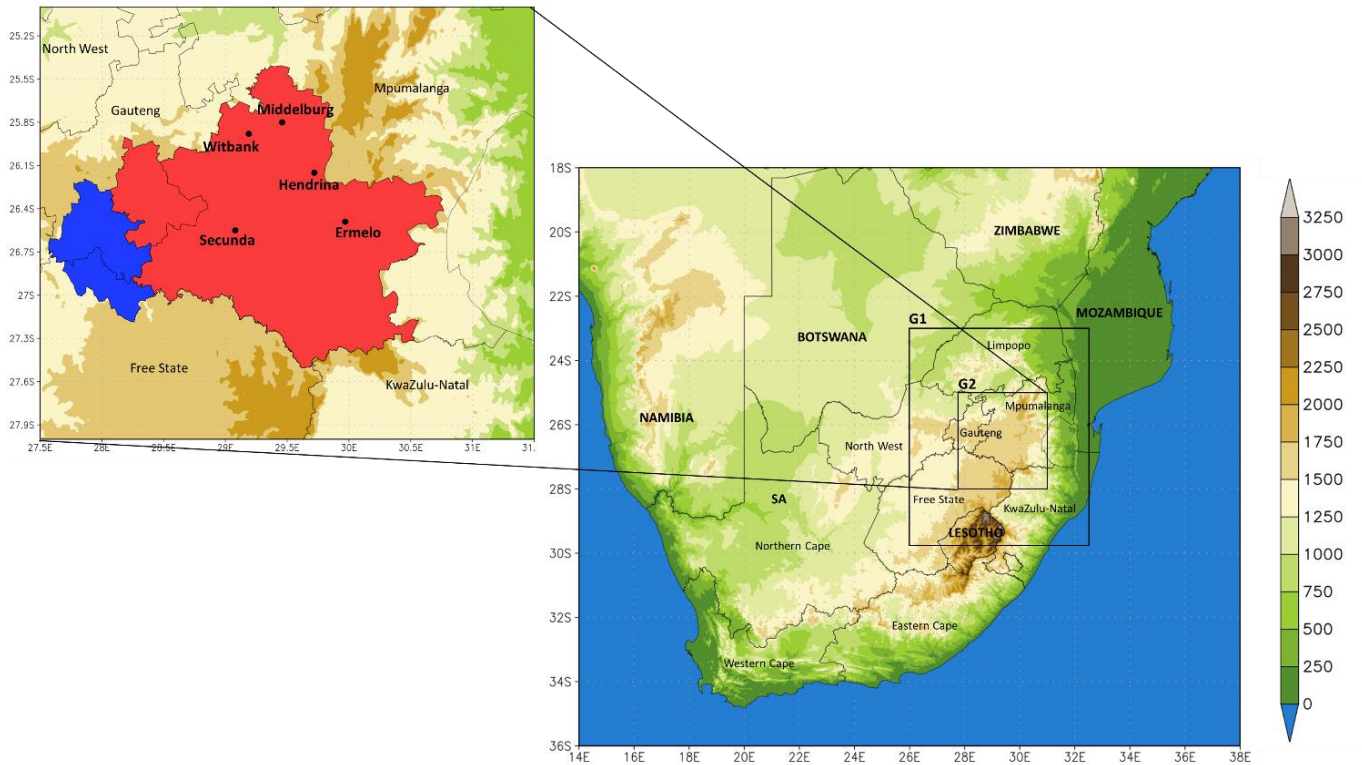


Figure 1. Domains for CAMx model simulations over South Africa (G1 = Grid 1; G2 = Grid 2). The scale indicates elevation in metres above sea level. The insert shows locations of the air quality monitoring stations used for the CAMx model evaluation. Outlines of relevant priority areas, HPA (red) and VTAPA (blue), are indicated on the insert. Spatial resolutions of G1 and G2 are approximately 6 km and 2 km, respectively.

The WRF-ARW model (Version 3.8.1) was used to produce meteorological input for the CAMx air quality model. Four experimental setups of the WRF-ARW model were run for June and November 2016 using different combinations of PBL and surface-layer schemes (SLSSs), as presented in Table 1. The main difference between the considered PBL schemes is closure type. The YSU and ACM schemes make use of non-local closure, while MYJ and MYNN use local closure. Briefly, this means that the YSU and ACM schemes take numerous atmospheric levels into account when representing vertical mixing in the PBL, while in the MYJ and MYNN schemes, vertical mixing at a certain level is only affected by the atmospheric levels with which they are in direct contact (Cohen *et al.*, 2015).

Other than the above-mentioned PBL and SLS schemes, the WRF-ARW model input data (land surface and initial and boundary conditions), parameterisation schemes for physics options, domains and resolution for the considered spring and winter simulations are identical. Consequently, any differences in pollutant concentrations between CAMx model simulations can be attributed to the PBL and SLS parameterisation schemes. The WRF-ARW model setup, and the verification and assessment of results from the WRF-ARW model runs, are explained in detail in De Lange *et al.* (2021). Briefly, the model was configured with three

domains of 18, 6 and 2 km. Input for initial and boundary conditions for the WRF-ARW was the six-hourly Climate Forecast System Version 2 (CFS v2) (Saha *et al.*, 2011) data at a $0.5^\circ \times 0.5^\circ$ grid resolution (0.2° for surface parameters) from the National Centers for Environmental Prediction (NCEP).

Land Surface Model (LSM) input data are from the static geographical dataset provided by WRF-ARW model developers. The majority of this global dataset was derived from the Moderate Resolution Imaging Spectroradiometer (MODIS) instrument and is based on 2001–2010 observations (Broxton *et al.*, 2014). This is the default dataset for the version of the WRF-ARW model used here (Zhang *et al.*, 2019).

The WRF-ARW simulations were configured with parameterisation schemes as presented in Table 2. Model simulations of pollutants are evaluated against observational data at five sites. De Lange *et al.* (2021) recommended using a local scheme for the Highveld region during winter. During spring, the clearly preferred scheme was MYJ.

Table 2. WRF-ARW model parametrisation scheme options (adapted from De Lange *et al.*, 2021).

Parameterisation	Scheme used	Reference
Microphysics	Single-moment six-class	Hong and Lim, 2006
Cumulus parameterisation scheme*	Kain-Fritsch	Kain, 2004
Longwave radiation	Rapid Radiative Transfer Model	Iacono <i>et al.</i> , 2008
Shortwave radiation	Rapid Radiative Transfer Model	Iacono <i>et al.</i> , 2008
Land surface model	4-layer Noah	Tewari <i>et al.</i> , 2004

* Only switched on for the 18 and 6 km domains

The CAMx model, Version 6.3, was used for air quality simulations; with a 0.06° (~ 6 km)-resolution parent domain, and a 0.02° (~ 2 km)-resolution nest (Figure 1). The CAMx utilises two-way nesting. Therefore, both domains in Figure 1 interact with each other. The 6 km-resolution WRF-ARW model output was used as input to the CAMx 6 km domain, and the same for the 2 km domain. The meteorological output from the WRF-ARW was processed through the WRF CAMx interface program for input into CAMx. The meteorological inputs for CAMx are provided on an hourly basis, and include the following: vertical grid structure (number of vertical layers and the vertical grid definition), horizontal wind components, surface temperature, pressure, humidity, water vapour, vertical diffusivity, cloud optical depth, precipitation and snow cover. Land use, topography and Leaf Area Index (LAI) are also required inputs (ENVIRON, 2016). For this study, these were derived from WRF-ARW through WRF CAMx. MOZART-4 Global Chemical Transport Model (GCTM) (Emmons *et al.*, 2010) output

was used for the CAMx initial and boundary conditions of the parent domain (Figure 1; Grid 1). Local time (LT) for the domain is universal time coordinated (UTC) +2.

Hourly emissions are input into CAMx with each source sector varying temporally according to an appropriate seasonal and diurnal profile (except for industrial emissions). The non-methane VOC emissions are speciated for the Carbon Bond 05 chemistry scheme (Yarwood et al., 2005), which was used in CAMx for treating gas phase chemistry. The CF scheme was used for treating aerosol size distributions. Aerosols of differing sizes (coarse and fine) are grouped and distributed via the CF scheme. Primary species are then modelled as either fine (PM_{2.5}) or coarse (PM₁₀), while secondary chemically formed species are modelled as fine particles (ENVIRON, 2016). For more detail regarding the chemistry mechanisms in the CAMx model, please refer to the user's manual available at www.camx.com. There are 29 vertical levels in the CAMx model run, and the height of the first few vertical layers, in which tall stacks would occur, are on average 28 m, 97 m, 192 m, and 314 m, across the domain. Pollutant concentrations were extracted at the first model level and are representative of an average over the level.

In addition to meteorological parameters, an emissions inventory is required for the CAMx model run. Data from a Highveld emissions inventory (for 2016) is used as input for both CAMx model domains (Figure 1). The inventory includes estimates for natural (biogenic volatile organic compounds (VOCs) and biomass burning) and anthropogenic (industry, residential fuel combustion, on-road vehicles and ammonia (NH₃) from an agricultural fertilizer application) emissions of CO, NO_x, non-methane VOCs, PM with an aerodynamic diameter $\leq 10 \mu\text{m}$ (PM₁₀), PM_{2.5}, SO₂, and NH₃.

Hourly emissions are input into CAMx with each source sector varying temporally according to an appropriate seasonal and diurnal profile (except for industrial emissions). The non-methane VOC emissions are speciated for the Carbon Bond 05 chemistry scheme (Yarwood *et al.*, 2005) used in CAMx for this study. The Council for Scientific and Industrial Research (CSIR) developed this emission inventory for the Highveld Health Study through funding from the South African Department of Environmental Affairs, Forestry and Fisheries (DEFF).

3. Data and model evaluation

3.1 Measured pollutant concentration data

This study focuses on evaluating the simulated pollutant concentration outputs from the CAMx model against measured data from monitoring stations across the HPA. The pollutants of interest include NO₂, O₃, PM_{2.5}, PM₁₀ and SO₂.

The pollutant monitoring stations that were used in this study are shown in Table 3. The monitoring stations at these sites are owned by DEFF, and the data is provided by the South African Weather Service (SAWS). Table 3 summarises the availability of pollutant concentration data after the quality control procedure. Data quality control includes the removal of unrealistic jumps or peaks in concentrations, negative values and periods of repeated values. Repeated values were identified as periods where pollutant concentration values were exactly the same for two or more hours in a row (US EPA, 2017; Zahumensky, 2004), except where applicable for O₃, which can be consistently low in the evenings. The selected sites are all in the HPA and are impacted on by a range of sources.

Table 3. Air pollution monitoring stations used for evaluation. Data available refers to the percentage of usable data hours after quality control. Sites where data availability was less than 70% for a certain pollutant are underlined. Pollutants with less than 70% availability after quality control were not considered for the model comparison.

Station name	Station classification	Latitude and longitude	Elevation	Data available per pollutant (June 2016)	Data available per pollutant (November 2016)
Ermelo	Low-income, residential, industrial, traffic	-26.493 °S, 29.969 °E	768 m	NO ₂ (52%) O ₃ (95%) PM _{2.5} (31%) PM ₁₀ (31%) SO ₂ (95%)	NO ₂ (33%) O ₃ (71%)* PM _{2.5} (99%) PM ₁₀ (99%) SO ₂ (99%)
Hendrina	Middle-class, residential, industrial	-26.151 °S, 29.716 °E	1 675 m	NO ₂ (100%) O ₃ (98%) PM _{2.5} (100%) PM ₁₀ (99%) SO ₂ (100%)	NO ₂ (100%) O ₃ (100%) PM _{2.5} (100%) PM ₁₀ (99%) SO ₂ (95%)
Middelburg	Middle-class, residential, industrial	-25.796 °S, 29.463 °E	1 509 m	NO ₂ (100%) O ₃ (1%) PM _{2.5} (98%) PM ₁₀ (93%) SO ₂ (100%)	NO ₂ (90%) O ₃ (98%) PM _{2.5} (99%) PM ₁₀ (99%) SO ₂ (0%)
Secunda	Low-income, residential, industrial	-26.548 °S, 29.080° E	1 575 m	NO ₂ (0%) O ₃ (87%) PM _{2.5} (87%) PM ₁₀ (87%) SO ₂ (87%)	NO ₂ (0%) O ₃ (95%) PM _{2.5} (100%) PM ₁₀ (100%) SO ₂ (99%)*
Witbank	Low-income, residential, industrial	-25.877 °S, 29.188 °E	1 527 m	NO ₂ (100%) O ₃ (100%) PM _{2.5} (100%) PM ₁₀ (100%) SO ₂ (26%)	NO ₂ (94%) O ₃ (0%) PM _{2.5} (100%) PM ₁₀ (100%) SO ₂ (75%)

An investigation of the hourly O₃ data for Middelburg during November (discussed in section 4.2) indicated a possible O₃ instrument fault during the first half of the month. Therefore, all presented statistics, diurnal

variation and bias plots for O₃ at Middelburg during November only considers data from Day 15 onwards. The O₃ concentrations at Ermelo during November are expected to be higher, and to peak in spring (Lourens *et al.*, 2011), but this is not seen at Ermelo, and it is not clear why. Therefore, the O₃ data for November is indicated with an asterisk (*) to highlight the fact that the monitored data is irregular. The SO₂ data at Secunda for November is also considered suspect, as explained in section 4.7. This data is also indicated with an asterisk (*).

3.2 Model evaluation

The performance when using different PBL schemes to drive CAMx and thus simulate surface-level pollutant concentrations was assessed by comparing simulated concentrations of NO₂, O₃, PM₁₀, PM_{2.5} and SO₂ with concentrations measured at the five stations (Figure 1) in the HPA. Statistical parameters, including mean, standard deviation, mean absolute error, mean error and Pearson product-moment correlation coefficient (R), were considered during model evaluation.

The standard deviation is calculated to compare the amount of variation or spread within the observed and simulation data. Mean error or bias is calculated as the difference between simulated and observed concentration, therefore a positive mean error is an indication of pollutant concentrations being over-estimated by the model simulation. For mean absolute error, the absolute value of the mean error is taken. Mean absolute error gives an indication of the average magnitude of error, while mean error includes an indication of the direction of the average error (positive or negative). The Pearson product-moment correlation coefficient is calculated to show the strength and direction of the relationship between simulated and observed pollutant concentrations. The strength of the absolute value of R can indicate weak (R = 0.1 to 0.29), moderate (R = 0.30 to 0.49) or strong (R = 0.50 to 1.0) relationships (Cohen, 1988).

4. Results

4.1 Comparisons of model and observations for NO₂

Observed average hourly NO₂ concentrations (measured in parts per billion (ppb)) show two diurnal peaks during June (Figure 2; left) at all stations investigated. Concentrations for November (Figure 3; left) show similar peaks (05 LT and 19 to 20 LT), but Hendrina shows a unique diurnal pattern, with NO₂ concentrations elevated throughout most of the day. Venter *et al.* (2012) found a similar diurnal pattern of two diurnal peaks in the Highveld region of South Africa. Two peaks generally indicate an increase in local emission sources, such as from the domestic combustion of solid fuels for cooking and heating or increased emissions from vehicle traffic.

Hendrina's diurnal pattern looks different as the station may be located within the path of plumes from a coal-fired power station, which is considered a large source of NO₂. Pollutants from tall stacks are emitted above the night-time surface inversion during spring, as this inversion breaks up in the morning. The trapped pollutants are mixed at the surface and lead to a peak in surface-level pollutants (Venter *et al.*, 2012). Another possible explanation for the diurnal pattern seen at Hendrina is that the station is located at a school, and midday traffic contributes to NO₂ concentrations. Diurnal variations are reasonably well simulated in terms of pattern during November (Figure 3; left), but these patterns were more accurately simulated during June (Figure 2; left). November biases are not as large as during June, and are predominantly less than 10 ppb throughout the day (Figure 3; right). NO₂ concentrations are largely the same during June and November, except for the likely contribution of domestic combustion for heat, and unfavourable meteorological conditions during June.

During June, the average observed and simulated NO₂ concentrations for all sites were of similar magnitude (Table 4), and average simulated concentrations and standard deviations are similar between schemes, especially at Witbank where YSU, MYJ, MYNN and ACM produced average concentrations of 17.47, 17.56, 17.05 and 17.33 ppb, respectively. All schemes under-estimated the averages and standard deviations. The schemes that produced the largest average concentrations and standard deviations are thus considered to be the best-performing schemes: MYJ produced the largest averages and standard deviations at the majority of sites, followed by MYNN. As with June, the average observed and simulated NO₂ concentration during November were on the same scale in terms of magnitude (Table 6). All schemes under-estimated averages during November, but not considerably. For example, the average observed concentration at Hendrina was 8.36 ppb, while the simulations produced an average of 5.61 ppb. MYNN performed best in terms of averages and standard deviations at Hendrina, while MYJ performed best at Middelburg, and YSU performed best at Witbank.

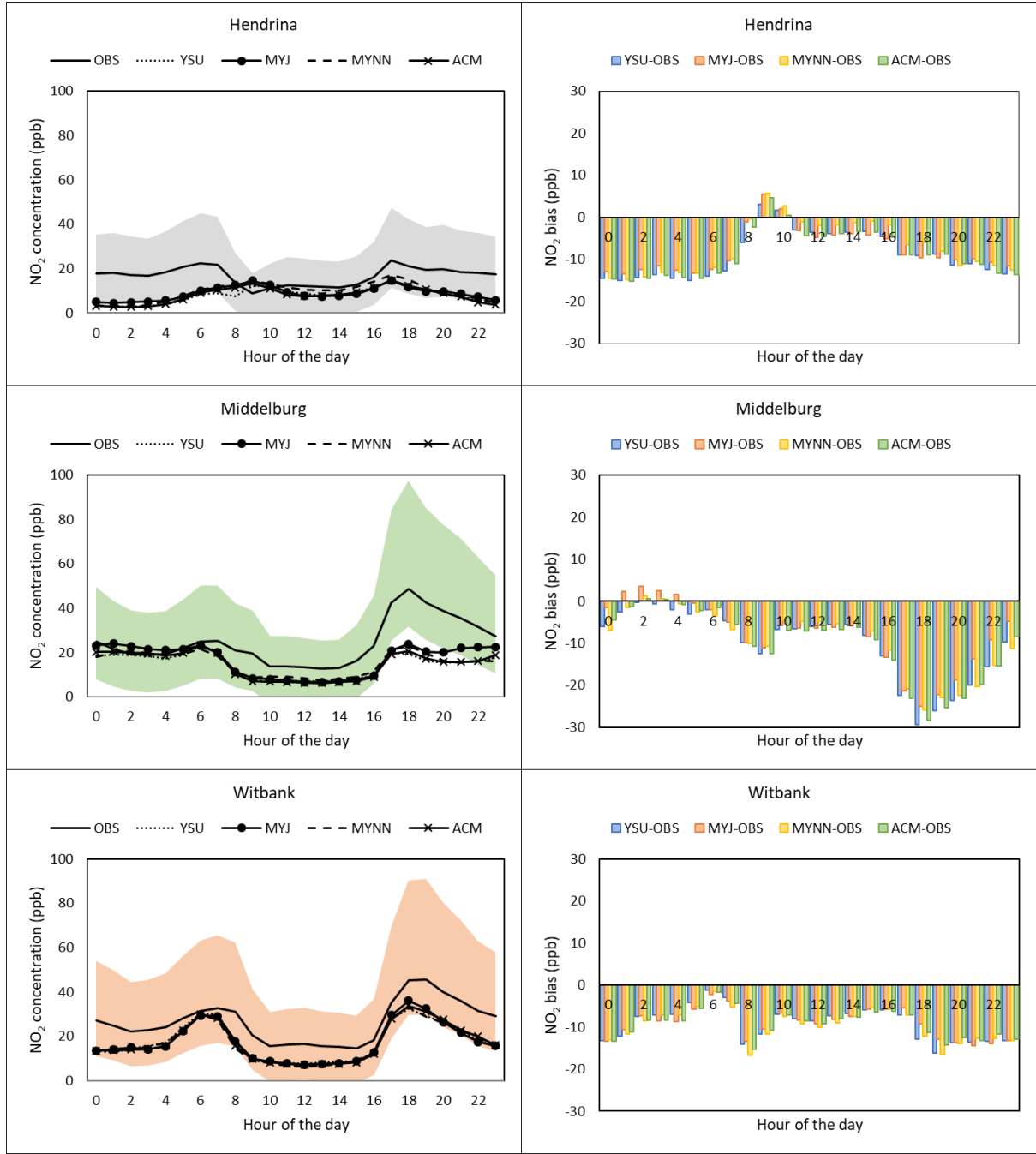


Figure 2. Average hourly NO₂ observed and simulated concentration for each of the sites (left), and average hourly bias during June (right). Average standard deviation from observed values is shaded on the diurnal variation plots.

At Middleburg, NO₂ concentrations are well simulated throughout the early morning in June, with average hourly biases less than 10 ppb from 00 to 07 LT (Figure 2; right). Thereafter, biases become much larger as all schemes under-estimate midday and afternoon concentrations. The average diurnal variation of NO₂ is well simulated at Witbank, but all schemes under-estimate concentrations throughout the day. Since similar simulations were produced by the different schemes, there is not a lot of variation between mean absolute error results for June (Table 5). MYJ performed best, but both local schemes did well on average

across the sites, with the lowest mean absolute errors. All average biases for the period were negative, with NO₂ concentrations only being over-estimated on occasion (Figure 2; right, and Figure B1). Once again, MYJ (followed by MYNN) performed best across the sites, producing the lowest biases on average.

The relationship between observed and simulated NO₂ concentrations is strong at Middelburg ($R > 0.52$) and Witbank ($R > 0.65$) during June, while only weak to moderate-strength correlations are produced at Hendrina (Table 5). In terms of correlations, on average across schemes, the different PBL schemes perform too similarly to identify a best-performing scheme.

Table 4. Observed (OBS) and simulated average and standard deviation of NO₂, O₃, PM_{2.5} and PM₁₀ for the period of June. Standard deviations are indicated in brackets next to the averages.

Pollutant	Sites	OBS	YSU	MYJ	MYNN	ACM
NO ₂	Hendrina	16.80 (12.4)	7.90 (8.0)	8.90 (8.0)	9.54 (9.1)	8.02 (7.5)
	Middelburg	24.62 (16.9)	14.49 (10.4)	16.76 (11.6)	15.30 (11.1)	14.63 (10.6)
	Witbank	26.69 (15.8)	17.47 (13.9)	17.56 (13.9)	17.05 (13.3)	17.33 (13.8)
O ₃	Ermelo	27.51 (13.0)	25.50 (9.4)	26.56 (10.1)	25.00 (10.0)	26.06 (9.3)
	Hendrina	19.50 (13.8)	26.92 (7.5)	27.91 (8.3)	25.94 (8.0)	27.37 (7.5)
	Secunda	25.93 (20.6)	23.95 (11.8)	24.35 (12.4)	23.80 (11.8)	24.26 (11.8)
	Witbank	18.68 (17.0)	20.67 (12.5)	22.15 (12.8)	21.28 (12.6)	21.13 (12.7)
PM _{2.5}	Hendrina	16.29 (12.5)	18.30 (16.7)	19.80 (20.0)	18.96 (17.6)	18.57 (18.9)
	Middelburg	18.53 (14.4)	19.42 (15.6)	18.56 (15.3)	20.17 (16.6)	17.66 (13.9)
	Secunda	74.77 (93.3)	36.37 (39.2)	39.97 (43.0)	34.23 (35.0)	34.45 (35.6)
	Witbank	45.95 (49.3)	26.64 (24.2)	25.61 (22.4)	26.38 (23.1)	26.00 (24.4)
PM ₁₀	Hendrina	31.87 (22.3)	22.61 (17.6)	24.02 (21.2)	23.81 (18.8)	22.61 (19.5)
	Middelburg	40.32 (48.0)	26.12 (20.0)	24.14 (19.0)	26.94 (20.4)	23.42 (18.0)
	Secunda	115.94 (144.8)	61.06 (86.4)	67.48 (95.8)	49.98 (58.9)	57.86 (77.9)
	Witbank	91.33 (91.4)	35.92 (29.0)	34.28 (26.7)	35.77 (27.9)	34.92 (29.2)
SO ₂	Ermelo	18.02 (18.6)	10.44 (10.1)	11.26 (10.2)	12.39 (11.2)	10.39 (9.6)
	Hendrina	13.85 (19.5)	9.96 (13.3)	10.57 (11.9)	12.69 (14.7)	9.88 (11.9)
	Middelburg	10.69 (15.7)	7.20 (10.0)	6.81 (9.2)	8.75 (11.5)	6.70 (8.5)
	Secunda	9.05 (13.4)	7.98 (12.9)	8.99 (13.3)	9.30 (17.6)	8.32 (14.0)

During November, in terms of mean absolute error, YSU performed well on average across sites, followed closely by MYJ (Table 7). MYJ outperformed the other schemes in terms of average bias across sites. The strength of relationships between observed and simulated NO₂ concentrations in November was much lower than during June. Correlations during November were very weak at Hendrina. This can be attributed to the fact that the model did not simulate diurnal pattern, along with mid-morning peak. Moderate correlations ($R = 0.30$ to 0.49) were found at most of the other sites and with the various setups. While correlations were low on average, YSU (followed by MYJ) performed reasonably well across all the considered sites.

Table 5. Average mean absolute error (MAE), bias and correlation (R) for each simulation for the period of June for each pollutant. Strong correlations ($R > 0.5$) are underlined.

Pollutant	Performance indicator	Site	YSU	MYJ	MYNN	ACM
	MAE	Hendrina	11.15	11.15	10.87	11.12
		Middelburg	13.16	11.67	12.76	12.88
		Witbank	12.10	12.26	12.06	12.23
		Hendrina	-8.89	-7.90	-7.25	-8.78

Pollutant	Performance indicator	Site	YSU	MYJ	MYNN	ACM
NO ₂	Bias	Middelburg	-10.13	-7.87	-9.33	-9.99
		Witbank	-9.22	-9.12	-9.64	-9.35
	R	Hendrina	0.36	0.27	0.31	0.32
		Middelburg	<u>0.52</u>	<u>0.58</u>	<u>0.54</u>	<u>0.56</u>
		Witbank	<u>0.65</u>	<u>0.66</u>	<u>0.66</u>	<u>0.65</u>
O ₃	MAE	Ermelo	7.92	8.05	8.50	7.83
		Hendrina	11.78	12.74	12.20	12.06
		Secunda	11.77	12.43	12.17	11.83
		Witbank	9.93	10.70	9.86	9.90
	Bias	Ermelo	-1.82	-0.80	-2.42	-1.27
		Hendrina	7.55	8.47	6.53	7.94
		Secunda	-1.84	-1.32	-1.93	-1.23
		Witbank	1.99	3.47	2.60	2.45
	R	Ermelo	<u>0.55</u>	<u>0.56</u>	<u>0.51</u>	<u>0.54</u>
		Hendrina	0.41	0.38	0.30	0.41
		Secunda	<u>0.68</u>	<u>0.62</u>	<u>0.64</u>	<u>0.67</u>
		Witbank	<u>0.62</u>	<u>0.61</u>	<u>0.66</u>	<u>0.65</u>
PM _{2.5}	MAE	Hendrina	10.65	11.18	10.98	11.31
		Middelburg	9.09	9.22	9.92	8.79
		Secunda	47.89	47.13	48.96	48.97
		Witbank	24.36	24.22	24.25	24.79
	Bias	Hendrina	2.02	3.51	2.67	2.28
		Middelburg	1.08	0.23	1.83	-0.69
		Secunda	-41.16	-38.39	-44.29	-42.67
		Witbank	-19.31	-20.33	-19.57	-19.94
	R	Hendrina	0.30	0.35	0.32	0.29
		Middelburg	<u>0.60</u>	<u>0.58</u>	<u>0.53</u>	<u>0.60</u>
		Secunda	<u>0.50</u>	0.48	<u>0.51</u>	0.46
		Witbank	<u>0.58</u>	<u>0.60</u>	<u>0.59</u>	<u>0.59</u>
PM ₁₀	MAE	Hendrina	16.98	17.20	17.33	18.04
		Middelburg	20.97	21.58	21.30	21.72
		Secunda	90.36	88.80	87.87	91.55
		Witbank	60.52	60.68	60.10	60.83
	Bias	Hendrina	-9.33	-7.92	-8.11	-9.31
		Middelburg	-13.82	-15.98	-13.02	-16.58
		Secunda	-60.70	-56.62	-72.55	-63.29
		Witbank	-55.41	-57.05	-55.57	-56.41
	R	Hendrina	0.33	0.35	0.31	0.29
		Middelburg	0.32	0.25	0.27	0.32
		Secunda	0.25	0.26	0.29	0.21
		Witbank	0.48	<u>0.51</u>	0.49	0.49
SO ₂	MAE	Ermelo	11.42	11.38	11.48	11.13
		Hendrina	9.56	10.48	10.17	9.69
		Middelburg	6.70	6.49	6.51	6.50
		Secunda	7.16	8.31	7.64	7.43
	Bias	Ermelo	-7.18	-6.74	-5.57	-7.61
		Hendrina	-3.89	-3.28	-1.15	-3.97
		Middelburg	-3.51	-3.91	-1.97	-4.02
		Secunda	-2.08	-0.65	-1.29	-2.22
	R	Ermelo	<u>0.51</u>	0.48	0.47	0.49
		Hendrina	0.49	0.37	0.47	0.43
		Middelburg	<u>0.54</u>	<u>0.58</u>	<u>0.61</u>	<u>0.61</u>
		Secunda	0.27	0.17	0.31	0.26

Peaks and lows of NO₂ on an hourly basis are relatively well captured by the model simulations during June (Figure B1). Although the concentrations are commonly under-estimated (negative biases), their variation is captured, hence the strong correlations at Middelburg and Witbank (Table 5). It is interesting to note the drop in observed and simulated concentrations for all sites from 12 to 14 June. During this time, a high ridging behind a cold front caused cold, moist and windy conditions over the Highveld, resulting in favourable conditions for pollution dispersion. The model simulations during November (Figure B2) capture the

magnitudes of certain peaks in hourly NO_2 concentration, but the lows are very rarely reproduced. Observed lows are much higher than those simulated, and rarely drop close to 0 ppb. This could point to a constant elevated level of NO_2 at these sites, which is not captured by the model. The source of this background NO_2 is possibly not included in the emissions used as input.

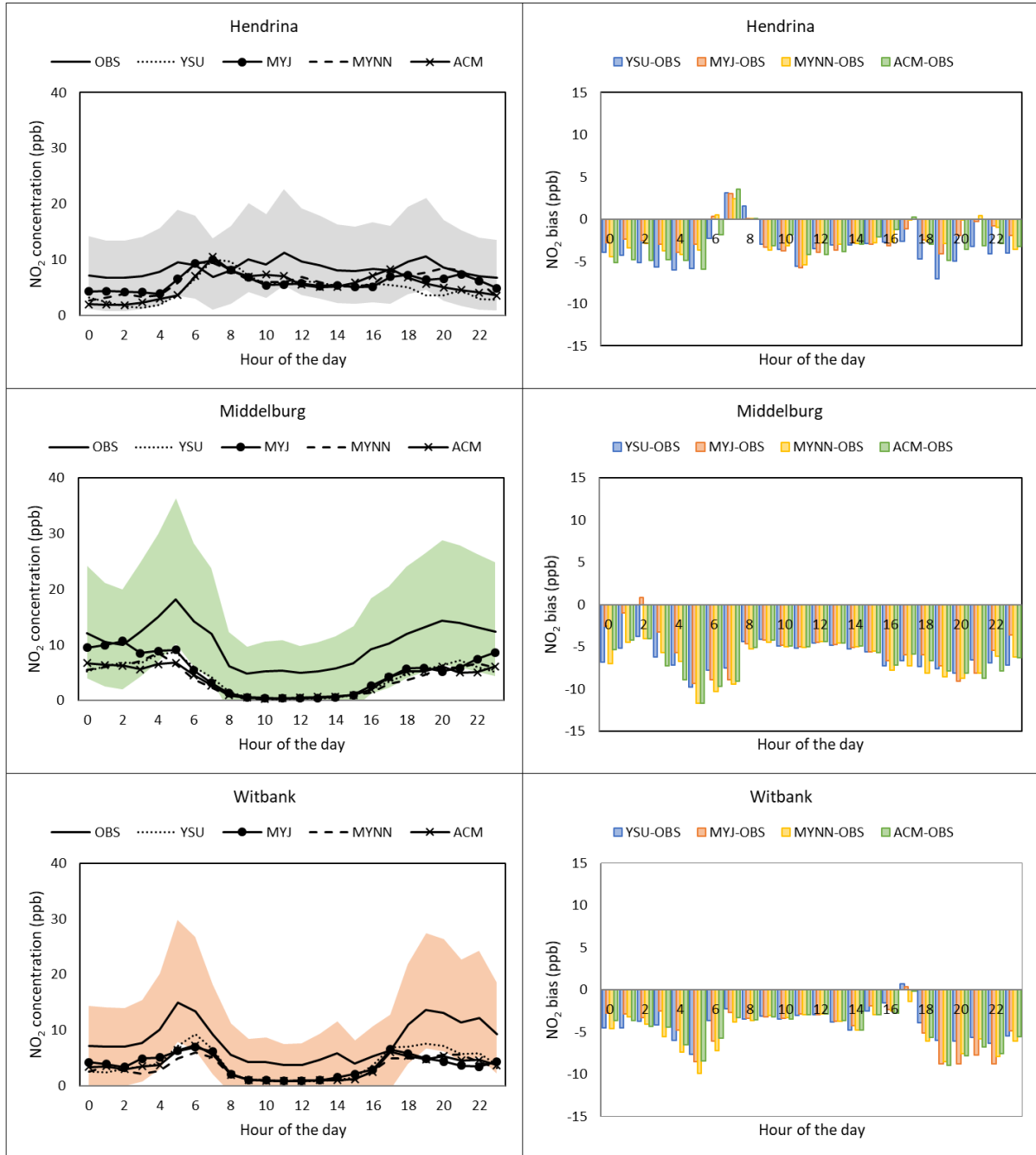


Figure 3. Average hourly NO_2 observed and simulated concentrations for each of the sites (left), and average hourly bias during November (right). Average standard deviation from observed values is shaded on the diurnal variation plots.

4.2 Comparisons of model and observations for ground-level O₃

Ambient O₃ concentrations (measured in ppb) are formed by precursor pollutants and photochemical processes. In addition, peaks in O₃ commonly occur near solar noon when ultraviolet radiation (UVR) is at a maximum (Lerche *et al.*, 2017). Time of maximum UVR varies between locations and seasons, but generally occurs at approximately 13 LT in the Highveld region (Cadet *et al.*, 2017; Venter *et al.*, 2012). Average observed O₃ concentrations peak at all sites between 14 and 15 LT during June (Figure A1; left). The timing of pollutant peaks is well simulated, although it is sometimes lower than observed. During November, the simulations did not capture the magnitudes of the observed O₃ concentration peaks well at Ermelo* and Hendrina (Figure B4). Hourly average biases show that all schemes over-estimate O₃ concentrations throughout the day for Ermelo* and Middelburg, while they under-estimate concentrations, on average, at Hendrina and Secunda (Figure A2; right).

As previously mentioned, O₃ concentrations at Ermelo and Middelburg during November appear irregular. In terms of Ermelo, O₃ concentrations are expected to be higher, and to peak in spring. This is not seen at Ermelo.

While the data have been included in all statistics and figures, it has been indicated by an asterisk (*) to highlight the fact that the monitored data are irregular. Observed concentrations for the first half of the month at Middelburg are low (average = 10.90 ppb), peak on 15 November, and then vary between much higher values (average = 24.89 ppb) (Figure B4). At this site, there is also a significant difference in average correlations before (R = 0.09) and after (R = 0.42) 15 November. This could indicate a possible instrument fault at the site for the first half of November. Therefore, all presented statistics (tables 6 and 7), diurnal variation and bias plots (Figure A2) for O₃ at Middelburg during November only consider data from 15 November.

Table 6. Observed (OBS), simulated average and standard deviation of NO₂, O₃, PM_{2.5}, PM₁₀, and SO₂ for the period of November. Standard deviations are indicated in brackets next to the averages.

Pollutant	Sites	OBS	YSU	MYJ	MYNN	ACM
NO ₂	Hendrina	8.36 (6.0)	4.77 (4.9)	6.02 (5.6)	6.05 (5.5)	5.33 (5.4)
	Middelburg	10.28 (8.0)	4.06 (4.8)	4.83 (6.3)	3.65 (5.2)	3.72 (4.6)
	Witbank	8.18 (7.0)	3.98 (4.7)	3.64 (4.3)	3.11 (3.7)	3.43 (3.7)
O ₃	Ermelo*	9.74 (7.4)	32.93 (10.1)	35.47 (10.6)	34.62 (9.2)	34.28 (10.6)
	Hendrina	41.72 (18.0)	30.65 (7.7)	31.96 (8.5)	30.72 (8.0)	31.61 (8.3)
	Middelburg	24.89 (11.6)	30.31 (8.2)	30.78 (9.0)	31.32 (7.7)	31.97 (7.5)
	Secunda	35.27 (19.6)	27.76 (11.4)	27.90 (12.8)	27.76 (12.3)	29.72 (11.9)
PM _{2.5}	Ermelo	19.32 (19.3)	18.17 (22.7)	18.55 (24.2)	14.78 (13.9)	17.69 (23.5)
	Hendrina	10.69 (6.4)	7.96 (7.6)	8.49 (8.3)	8.28 (6.6)	8.00 (6.6)
	Middelburg	4.97 (3.7)	4.89 (2.6)	4.96 (2.5)	5.53 (2.6)	5.11 (2.7)
	Secunda	14.99 (9.3)	8.79 (6.1)	8.07 (4.5)	8.16 (3.9)	8.59 (6.2)
	Witbank	10.27 (7.2)	6.38 (3.7)	6.21 (3.3)	6.64 (3.1)	6.23 (3.3)
PM ₁₀	Ermelo	36.28 (33.1)	19.86 (23.0)	20.25 (24.5)	16.43 (14.0)	19.49 (23.8)
	Hendrina	21.49 (22.0)	9.49 (7.9)	9.95 (8.6)	9.87 (6.9)	9.77 (7.1)
	Middelburg	8.48 (8.7)	5.89 (3.7)	5.93 (3.2)	6.56 (3.3)	6.16 (3.5)
	Secunda	28.60 (23.8)	18.11 (20.4)	14.47 (12.5)	14.34 (10.8)	16.66 (19.8)

	Witbank	22.68 (19.9)	8.04 (4.5)	7.65 (3.9)	8.15 (3.8)	7.79 (3.8)
	Ermelo	8.37 (10.7)	4.52 (4.8)	4.98 (5.2)	4.70 (4.4)	4.64 (5.1)
SO₂	Hendrina	10.11 (16.9)	6.95 (9.9)	8.02 (8.6)	8.70 (8.7)	7.32 (9.2)
	Secunda*	4.38 (9.0)	9.44 (11.2)	11.49 (12.2)	11.50 (15.0)	8.51 (10.6)
	Witbank	7.00 (6.0)	2.46 (3.9)	2.34 (4.0)	2.07 (3.4)	1.94 (2.9)

* Anomalous data

Average observed and simulated O₃ concentrations are of a similar magnitude during June (Table 4). For instance, the observed average concentration at Ermelo is 27.51 ppb for the period, while average simulated concentrations vary between 25 and 26.56 ppb. Considering standard deviations, the observed concentrations vary more than the simulated concentrations. Schemes again performed similarly, and no scheme successfully captured this variation in concentration, but MYJ produced averages nearest to the observed concentrations at two of the four stations. Observed and simulated O₃ concentrations differed considerably during November. For instance, the average observed concentrations at Ermelo* were more than 20 ppb less than the simulated concentrations (Table 6). At Hendrina, these concentrations were more comparable (average observed = 41.72 ppb; average simulated = 31.07 ppb). Similar to June, O₃ averages were not consistently over- or under-simulated across sites during November. Not considering Ermelo*, YSU, MYJ and MYNN each produced average O₃ concentrations closest to the observed concentrations at one of the sites.

Diurnal variation of O₃ at Ermelo was very well simulated during June, with all schemes producing average negative biases of less than 3 ppb (Figure A1; right). The largest biases were found at Secunda, which displayed significant under-estimation of the daily peak concentrations (09 to 18 LT), whereas Hendrina also displayed large biases, with an over-estimation of early morning and late afternoon concentrations for June (Figure A1; left). The model tends to simulate higher evening ozone levels; particularly for Hendrina and Witbank. A likely reason is that evening NO (which tracks NO₂ in the model) is under-estimated, leading to the suppression of evening titration and thus higher ozone levels. While concentrations at certain sites were better reproduced than at others, schemes produced very similar concentrations – and consequently biases – at the different sites. During November (Figure A2; left), O₃ peaks were observed between 15 and 16 LT. The O₃ concentrations for June and November were in a similar order of magnitude for Hendrina and Secunda, but this was not true at Ermelo, where November concentrations were lower than June concentrations. The observed data at Ermelo during November looks anomalous, since O₃ concentrations during spring should be higher than or at least similar to concentrations in winter. Other sites are not comparable in the same manner as data was not available during both months.

While schemes produced very similar results at the considered sites during June in terms of mean absolute error (Table 5), YSU and ACM outperformed the other schemes by a small margin, yielding the lowest mean absolute errors across sites on average. Average biases for the period are mostly low (< 7 ppb), negative at Ermelo and Secunda, and positive at Hendrina and Witbank. MYJ (followed by YSU) produced the lowest biases on average across sites. Correlations between observed and simulated O_3 show good results for June. This can be attributed to the fact that the model reproduced diurnal variation relatively well (Figure A1; left). Schemes show strong relationships with observed concentrations at Ermelo, Secunda and Witbank, as well as medium-strength relationships ($R = 0.30$ to 0.41) at Hendrina. On average, across all sites, YSU and ACM have the strongest correlations.

Table 7. Average mean absolute error, bias, and correlation (R) for each simulation for the period of November for each pollutant. Strong correlations ($R > 0.5$) are underlined.

Pollutant	Performance indicator	Site	YSU	MYJ	MYNN	ACM
NO_2	MAE	Hendrina	6.09	6.19	6.17	6.15
		Middelburg	7.41	7.20	7.74	7.77
		Witbank	5.50	5.78	5.83	5.75
	Bias	Hendrina	-3.59	-2.34	-2.32	-3.03
		Middelburg	-6.27	-5.38	-6.63	-6.55
		Witbank	-4.07	-4.42	-4.96	-4.70
	R	Hendrina	0.04	-0.04	-0.02	0.03
		Middelburg	0.33	0.35	0.35	0.25
		Witbank	0.38	0.29	0.32	0.32
	MAE	Ermelo*	22.51	25.11	24.52	23.97
		Hendrina	15.87	15.52	16.25	15.60
		Middelburg	9.79	9.70	10.09	10.71
		Secunda	15.86	15.76	15.59	14.83
O_3	Bias	Ermelo*	22.41	25.04	24.44	23.76
		Hendrina	-11.08	-9.77	-11.00	-10.11
		Middelburg	5.42	5.89	6.43	7.07
		Secunda	-7.39	-7.49	-7.52	-5.71
	R	Ermelo*	<u>0.53</u>	0.48	0.49	0.40
		Hendrina	0.34	0.33	0.31	0.31
		Middelburg	0.17	0.21	0.18	0.21
		Secunda	0.41	0.46	0.45	0.45
	MAE	Ermelo	15.91	15.18	12.85	14.49
		Hendrina	6.92	6.75	6.62	6.76
		Middelburg	3.13	3.44	3.20	3.25
		Secunda	9.10	8.80	8.61	8.98
$PM_{2.5}$	Bias	Witbank	5.18	5.24	4.89	5.22
		Ermelo	-1.13	-0.76	-4.53	-1.61
		Hendrina	-2.72	-2.19	-2.41	-2.69
		Middelburg	-0.09	-0.02	0.55	0.12
	R	Secunda	-6.20	-6.92	-6.83	-6.40
		Witbank	-3.89	-4.06	-3.63	-4.04
		Ermelo	0.26	0.31	0.35	0.29
		Hendrina	0.08	0.06	0.02	0.04
		Middelburg	0.10	-0.06	0.08	0.08
		Secunda	0.09	0.09	0.10	0.05
		Witbank	0.37	0.30	0.38	0.27
PM_{10}	MAE	Ermelo	27.58	27.06	25.58	26.78
		Hendrina	15.37	15.11	14.84	14.87
		Middelburg	5.46	5.80	5.45	5.56
		Secunda	24.43	21.00	21.20	23.95
	Bias	Witbank	15.65	15.93	15.33	15.76
		Ermelo	-16.38	-15.99	-19.82	-16.77
		Hendrina	-11.99	-11.53	-11.61	-11.72

Pollutant	Performance indicator	Site	YSU	MYJ	MYNN	ACM
SO ₂	R	Middelburg	-2.60	-2.55	-1.92	-2.32
		Secunda	-10.49	-14.13	-14.26	-11.94
		Witbank	-14.65	-15.03	-14.53	-14.89
		Ermelo	0.14	0.18	0.21	0.16
		Hendrina	-0.02	-0.05	-0.05	-0.05
		Middelburg	0.10	0.00	0.13	0.07
		Secunda	-0.11	-0.08	-0.11	-0.14
		Witbank	0.29	0.24	0.36	0.21
	MAE	Ermelo	6.44	6.85	6.38	6.87
		Hendrina	10.14	10.97	10.92	10.29
		Secunda*	8.77	10.79	11.12	8.33
		Witbank	5.65	5.98	5.69	5.74
	Bias	Ermelo	-3.87	-3.39	-3.67	-3.73
		Hendrina	-2.98	-2.06	-1.47	-2.56
		Secunda*	5.06	7.14	7.16	4.14
		Witbank	-4.46	-4.67	-4.68	-4.93
	R	Ermelo	0.37	0.25	0.33	0.21
		Hendrina	0.14	0.06	0.09	0.10
		Secunda*	0.14	0.03	0.04	0.01
		Witbank	0.11	-0.04	0.15	0.08

* Anomalous data

Considering mean absolute error results during November, all schemes produced similar results, which led to a similar magnitude of error across schemes and sites (Table 7). On average across all sites (except Ermelo*), MYJ produced marginally better results than the other schemes, while ACM produced the smallest average biases. Correlations are very similar between schemes during November. Excluding Ermelo*, MYJ again marginally outperformed the other schemes.

Table 8. Observed (OBS) and simulated average daily peak concentrations of O₃ for the period of June and November.

Period	Site	OBS	YSU	MYJ	MYNN	ACM
June 2016	Ermelo	41.95	37.34	38.35	37.34	38.40
	Hendrina	39.89	36.33	37.30	35.24	36.78
	Secunda	59.04	39.62	41.01	39.45	40.43
	Witbank	47.94	38.06	38.94	37.98	38.92
November 2016	Ermelo*	20.29	48.90	51.06	49.06	50.26
	Hendrina	67.58	41.19	42.78	41.56	43.29
	Middelburg	39.87	39.78	40.25	38.96	40.58
	Secunda	57.52	43.16	45.11	44.01	45.30

* Anomalous data

The average daily peak concentrations for June and November are presented in Table 8. Differences between average observed and simulated peaks vary between 8.71% at Hendrina, and 32.03% at Secunda during June. In terms of reproducing daily peak O₃ values, MYJ and ACM performed best, only under-estimating these peak values by approximately 16% on average across all sites during June. Reproducing daily peak O₃ values was less successful during November, especially at Ermelo*, Hendrina and Secunda. All schemes reproduced peaks at Middelburg very well, with an average percentage difference of only 1.3% across schemes.

Hourly time series plots (Figure B3) for June show that the simulations are reproducing hourly variations in observed concentrations. For example, the simulations reproduced the elevated O₃ levels observed at Ermelo between 11 and 14 June. While some characteristics of the pollutant concentrations are well reproduced, the simulations do not capture large spikes (e.g. Secunda) or lows (e.g. Hendrina) in concentrations at times. Figure B4 shows time series plots of O₃ concentration at all sites for November.

4.3 Comparisons of model and observations for PM_{2.5}

Observed PM_{2.5} concentrations, which are measured in micrograms per cubic meter (µg/m³), show very distinct morning and afternoon peaks during June (Figure A3; left). These morning and afternoon peaks may be primarily attributed to domestic fuel combustion and/or vehicular traffic. November PM_{2.5} concentrations also show morning and afternoon peaks at all sites, but to differing levels between sites (Figure A4; left). In addition to these peaks, during this period, average hourly concentrations remain somewhat elevated throughout the day and evening during November at the sites considered. The two distinct concentration peaks are characteristic of the diurnal cycle of PM_{2.5}, as De Lange *et al.* (2019) previously found in the Highveld region. The most noticeable difference between November and June is the significantly lower levels of PM_{2.5} in the observed and simulated concentrations during November.

This seasonal difference exhibited by both observed and simulated concentrations is attributed to seasonally varying emissions, as well as air dispersion potential, between the two seasons. Since higher temperatures occur in the study region during November, domestic fuel combustion for heat should not contribute as much to emissions (Hersey *et al.*, 2015). Meteorological conditions are also more favourable for pollution dispersion during spring (Tyson *et al.*, 1988).

Considering averages for June, observed and simulated concentrations at some sites are of differing magnitudes (Table 4). Concentrations are slightly over-estimated at Hendrina and Middelburg, and under-estimated to a larger degree at Secunda and Witbank. Hourly time series plots for June (Figure B5) support this statement. Sites with higher average PM_{2.5} concentrations also have larger standard deviations. The different schemes perform similarly in simulating average PM_{2.5} concentrations and produce similar standard deviations. MYJ simulated the most accurate average concentrations for June at two (Middelburg and Secunda) out of four sites, while YSU performed best at each of the remaining sites. ACM simulated standard deviation well at Middelburg.

Observed and simulated PM_{2.5} concentrations are more comparable, and of a similar magnitude, during November (Table 6). For instance, the average observed concentration at Hendrina is 10.69 µg/m³ for the period, while the simulated concentration is 8.18 µg/m³, on average. Once again, the model simulates the average concentration at Middelburg well, as the simulated concentration differs less than 1.00 µg/m³ from the observed average. Results between the different schemes are similar, but MYJ performed well across most of the considered sites.

The variation in the data contributes some interesting results. For instance, in the case of Ermelo, the standard deviation of simulated PM_{2.5} is larger than observed, except for one scheme (MYNN), where the standard deviation is lower. For the remaining sites, all schemes simulated similar standard deviations. Diurnal patterns are reproduced well at Middelburg during June, where correlations are strong and average errors are low (Table 5). Considering the strength of the relationship between the observed and simulated PM_{2.5} concentration, correlations are quite similar between the schemes. On average, MYJ (followed by YSU) had the strongest correlations on average across sites. In terms of mean absolute error for June (Table 5), as expected from the time series plots in Figure B5, the largest errors were observed at Secunda and Witbank, whereas all schemes produced mean absolute errors less than 10 µg/m³ for Middelburg. MYJ performed best across all sites on average with respect to mean absolute error and bias, followed by YSU.

Figure A3 presents average hourly PM_{2.5} concentrations (left), as well as bias (right), on a diurnal scale for June. It is interesting to note that the hours of the day during which biases are largest mostly coincide with the times of concentration peaks in the diurnal cycle. For instance, while the observed morning peak in concentrations at Witbank takes place between 05 and 10 LT, the peaks in bias take place between these same times. A larger peak in concentration is observed in the evening from 16 LT. Large biases are present during approximately the same hours. Similar patterns are present at all sites, but to differing degrees. As these peaks in the monitoring data are greatly impacted on by local emission sources, these large biases suggest that the emissions from these sources are under-estimated, or absent in the emissions inventory.

The largest variations between the different schemes occur during the morning and afternoon concentration peaks in June (Figure A3) and November (Figure A4). Since all schemes are presented with the same emission data, the differences in performance at some of the sites can be attributed to how processes, especially with respect to the PBL, are handled within the schemes. For instance, throughout June at Middelburg, during the

afternoon peak, MYNN simulates PM_{2.5} concentration to be the highest, followed by MYJ, YSU and ACM (Figure A3; right).

The diurnal variation of PM_{2.5} concentrations during November is reproduced well at Ermelo. A morning (04 to 07 LT) and afternoon (16 to 19 LT) peak is observed and nearly replicated (Figure A4; left). Biases are relatively small during the morning, but large during the evening. MYNN is the best-performing scheme in reproducing diurnal variation at Ermelo. This is because of the magnitude of the afternoon peak being simulated most accurately. While simulations are often very similar between schemes, when there is a difference, MYNN is normally the scheme that deviates the most. This deviation is especially noticeable in the evenings.

Considering simulation errors for November (Table 7), mean absolute errors are relatively small ($< 10 \mu\text{g}/\text{m}^3$) at Hendrina, Middelburg, Secunda and Witbank, while they are larger than $10 \mu\text{g}/\text{m}^3$ at Ermelo. The local scheme, MYNN, yields the smallest mean absolute error at most of the sites during this period. Except for some peaks in the observed concentrations, PM_{2.5} is reproduced relatively well at Middelburg during November with very low biases, ranging on average from $-0.02 \mu\text{g}/\text{m}^3$ (MYJ) to $0.55 \mu\text{g}/\text{m}^3$ (MYNN). The strength of the relationships between observed and simulated PM_{2.5} concentrations during November are mostly low, and quite similar between schemes. On average, MYJ and ACM produced the strongest correlations with observed concentrations across sites. The strongest correlations were found at Witbank, where YSU and MYNN produced the strongest correlations. MYJ (followed by YSU) produced the smallest biases on average across sites during this period.

4.4 Comparisons of model and observations for PM₁₀

Observed PM₁₀ concentrations (measured in $\mu\text{g}/\text{m}^3$), show two diurnal peaks during June (Figure A5; left). Morning peaks are present from 04 to 09 LT, and afternoon peaks from 16 to 21 LT, to differing degrees at all sites. Venter *et al.* (2012) found the same diurnal pattern in the Highveld region. The peaks in PM₁₀ concentration are likely due to sources such as domestic fuel combustion and vehicular traffic. PM₁₀ concentrations during November show a small morning (05 to 07 LT) and larger evening (19 LT) peak at Middelburg (Figure A6; left). The remaining sites reach a peak in PM₁₀ concentrations in the morning. Thereafter, concentrations continue to increase until a maximum daily level is reached between 16 and 19 LT. As with PM_{2.5}, there is a significant difference in pollutant concentration magnitudes between June and November, with decreased values in November. Causes of these differences include the reduction in domestic

fuel combustion sources during November, as well as the influence that favourable meteorological conditions can have on pollution dispersion.

Average PM₁₀ concentrations are under-estimated at all sites during June, and there are some large differences in magnitude between average observed and simulated concentrations (Table 4). For example, the average observed concentration at Secunda for the period was 115.94 µg/m³, while the simulated concentration averaged 59.10 µg/m³. Observed standard deviations for this site are also much larger than the simulated concentrations. The diurnal variation of PM₁₀ at the considered sites is well reproduced by the simulations (Figure A5; left), but, while the presence of pollutant peaks during June are captured, their magnitudes are not. This is very evident at Secunda where the afternoon peak in June is under-estimated by nearly 350 µg/m³.

A similar under-estimation is present in Witbank's afternoon peak, where concentrations are under-estimated by close to 200 µg/m³ on average (Figure A5; right). This suggests either the under-estimation of important PM₁₀ sources (e.g. domestic fuel combustion) or the absence of very localised sources (e.g. wind-blown dust from open fields) around these sites during June. At Hendrina, observed concentrations peak between 07 and 10 LT (at 45 µg/m³), and again between 17 and 20 LT (at 40 µg/m³). The morning peak is under-estimated and simulated earlier than observed, while the afternoon peak is over-estimated and simulated later than observed. The over-estimation of afternoon/evening PM₁₀ is most likely due to the simulated enhanced impact of domestic fuel combustion emissions from a township located less than 3 km from the Hendrina site due to model resolution, as detailed in the introduction.

While different schemes produced similar simulated concentrations during June, MYNN (followed by MYJ and YSU) produced the smallest average mean absolute error across the sites (Table 5). Average biases for the period are negative for all sites. MYJ, followed by YSU, produced the lowest biases on average across sites. The relationships between observed and simulated PM₁₀ concentrations are mostly weak to moderate, with some stronger correlations found at Witbank (Table 5). Although mean absolute errors are large at Witbank, correlations are strong because all schemes capture the diurnal pattern well. All schemes performed well in terms of correlations at Witbank because the simulated concentrations between the schemes were so similar. The two local schemes (MYJ and MYNN) performed well at all sites, except Middelburg, where the non-local schemes (YSU and ACM) produced slightly stronger correlations. When considering average correlations across sites, YSU produced the strongest relationships, followed closely by MYJ and MYNN.

Average observed and simulated PM₁₀ concentrations during November are of a similar magnitude at Middelburg, with some larger differences ($> 10 \mu\text{g}/\text{m}^3$) at the remaining sites (Table 6). Results between schemes are very similar at some sites (Hendrina, Middelburg and Witbank), while they are more variable at others (Ermelo and Secunda). This is also true in terms of standard deviations. The two local schemes yielded averages similar to those observed at most of the sites during November. While mean absolute errors are similar between schemes during November, the simulated concentrations produced by MYNN (followed by MYJ) led, on average, to the smallest mean absolute errors across all sites (Table 7). Average biases were relatively large ($>10\mu\text{g}/\text{m}^3$) and negative at all sites except Middelburg, where biases were small ($<-3 \mu\text{g}/\text{m}^3$). Very weak and sometimes negative correlations are found between observed and simulated concentrations at all sites except Witbank during November. While correlations are very weak, MYNN produced the strongest correlations on average across the sites considered during November.

Very weak correlations during November are clarified by hourly average diurnal variations (Figure A6), and hourly time series concentrations (Figure B6). While only one afternoon peak is observed at these sites (Figure A6; left), a morning and afternoon peak is simulated at most sites. Simulated concentrations at Middelburg do not show any peaks, rather a gradual increase in PM₁₀ concentrations from early morning until noon, and then a gradual decrease. Figure B6 shows the number of observed concentration peaks, which were not reproduced by the model simulations, but also frequent simulated peaks, which, in reality, did not take place. These uncaptured peaks are the reason for the large differences in average concentrations and standard deviations, large errors and low correlations found during November.

4.5 Comparisons of model and observations for SO₂

Observed SO₂ concentrations (measured in ppb) do not show a distinguishably common diurnal pattern among the different sites in June, but share some common features. In June, a morning (07 LT) and afternoon (18 LT) peak is visible at Ermelo (Figure 4; left). Concentrations at the other sites peak later, between 11 and 12 LT. An afternoon peak is also discernible at Secunda. These differences could mean that either different sources contribute to SO₂ concentrations at the different sites or tall stack emissions reach the surface at different times. Venter *et al.* (2012) found a similar singular mid-morning peak in the diurnal patterns of a site in the Highveld region. As previously mentioned, SO₂ concentrations at Secunda during November appear irregular. These data were included in all statistics and figures, and is indicated by an asterisk (*).

During November, some common features are visible in the diurnal cycle between sites (Figure 5; left). Ermelo, Hendrina and Secunda show peak concentration values between 10 and 11 LT, while Witbank's concentrations peak only slightly after 20 LT at night. Since morning and afternoon peaks are not present, tall stacks likely contribute to SO₂ peaks at about 11 LT. Emissions from these stacks are mixed downward in the daytime, contributing to SO₂ concentration peaks at the sites during November. The magnitudes of observed SO₂ concentrations are somewhat different between June and November, but not nearly as significantly different as some of the other pollutants considered. This may suggest that the sites are impacted on by SO₂ sources that are relatively constant between seasons.

Average observed and simulated SO₂ concentrations are of comparable magnitudes during June, with differences being less than 10 ppb for all simulations at all sites (Table 4). Compared to some of the other pollutants considered, averages are relatively well simulated and standard deviations are close to the observed values for SO₂ during June. For instance, the average simulated concentration at Secunda is 9.05 ppb, while simulations produced averages between 7.98 and 9.30 ppb.

MYNN produced averages and standard deviations closest to the observed values at Ermelo, Hendrina, and Middelburg, while MYJ produced these at Secunda. Observed and simulated average concentrations and standard deviations during November were also of a similar magnitude (Table 6). For instance, the observed SO₂ concentration at Hendrina was 10.11 ppb, while simulated average values varied between 6.95 and 8.70 ppb. As during June, differences between observed and simulated SO₂ concentrations for November are less than 10 ppb across all schemes and sites. All the different schemes produced an average most similar to the observed value. A best-performing scheme for all sites could therefore not be identified.

Diurnal variation of observed SO₂ during June was captured to some extent at all sites (Figure 4; left). Diurnal variation of SO₂ concentrations was not well reproduced during November. Although average biases are relatively low (less than 8 ppb for all schemes across all sites), the diurnal patterns are mostly not captured (Figure 5; left). Some visible differences in average hourly concentrations and biases were produced by the four schemes during November, with biases varying between schemes, especially at Secunda* (Figure 5; right). Mean average errors between schemes are similar for November, except for some larger differences between the local and non-local schemes at Secunda (Table 7). On average across all sites, the two non-local schemes, YSU and ACM, produced smaller mean absolute errors. In terms of bias and correlations, MYNN performed best, on average, across sites.

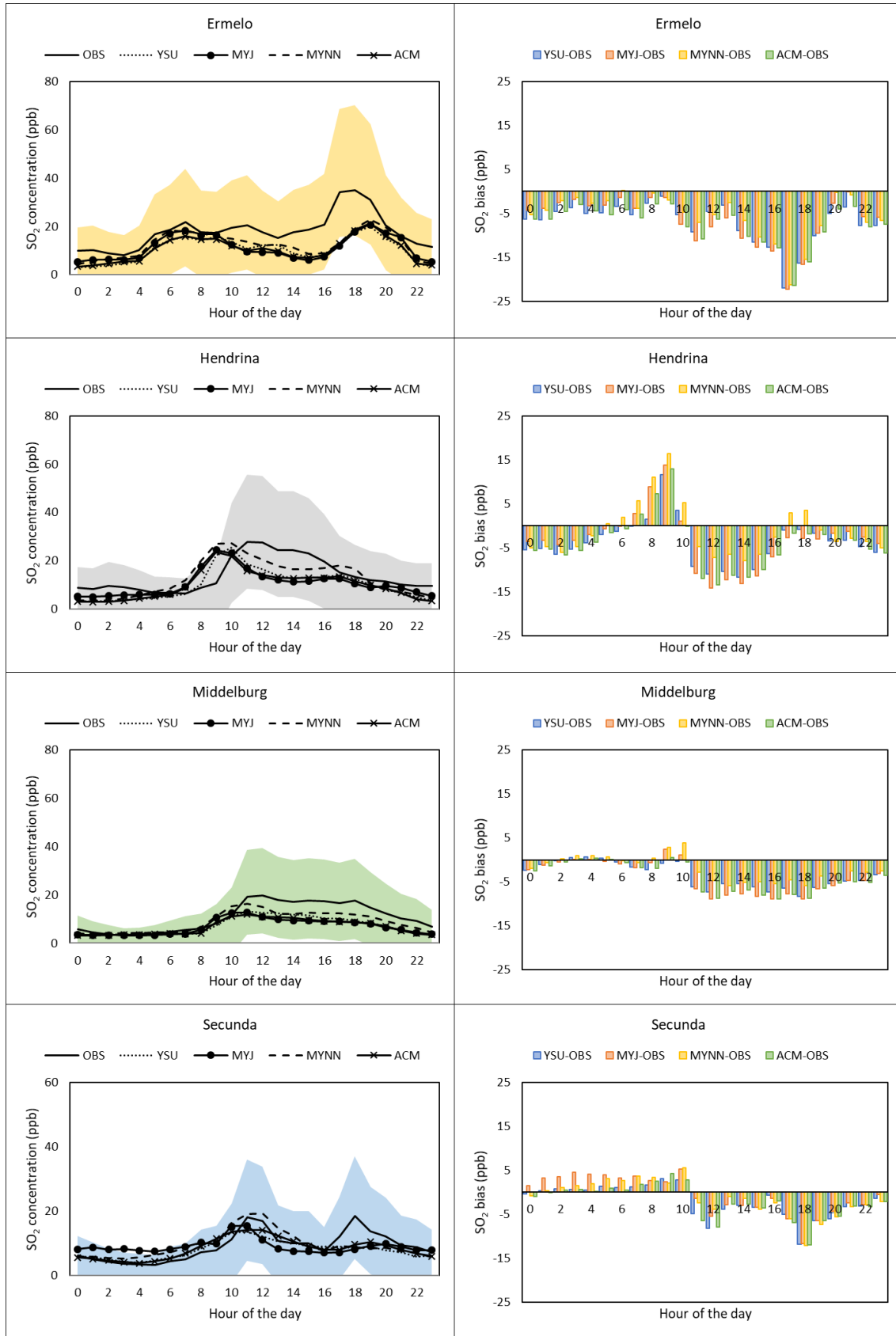


Figure 4. Average hourly SO₂ observed and simulated concentrations for each of the sites (left), and average hourly bias during June (right). Average standard deviation from observed values is shaded on the diurnal variation plots.

During November, there were some visible differences in average hourly biases produced by the four schemes compared to those produced during June (Figure 5; right). This was especially visible at Hendrina and Secunda*. While there were some discrepancies in the average hourly biases between schemes, when an average mean absolute error for the period is considered (Table 7), results between schemes again appeared very similar, with YSU and ACM having the smallest mean errors, on average, across sites. However, in terms of bias, the two local schemes, and MYNN in particular, were the best performers.

Although the diurnal variation of SO₂ concentrations at Hendrina was not captured well by the model setups during June (Figure 4; left), correlations at this site were not as low as would be expected, ranging between 0.37 and 0.49 (Table 5). This is because the general increase and decrease in simulated concentrations took place during the same time as they were observed. The relationship between observed and simulated SO₂ concentrations was strong at Middelburg because the diurnal variation was well captured at this site. When considering correlations across all sites, MYNN performed best on average, followed closely by both the local schemes.

For November, predominantly weak relationships are present across schemes and sites, except for some medium-strength relationships found at Ermelo for YSU ($R = 0.37$) and MYNN ($R = 0.33$) (Table 7). This is because, while the scale of simulated SO₂ is lower, the pattern of diurnal SO₂ variation is captured to some degree. While correlations are mostly weak and no scheme performed particularly well, considering correlations across all sites, YSU and MYNN performed best on average.

The hourly time series plots of June concentrations in Figure B9 show promising results with respect to how well hourly concentration levels are captured by the model simulations. Peaks and lows in concentrations are reproduced well in comparison to some of the other pollutants considered. Middelburg experienced a period of low SO₂ concentrations from 12 to 23 June, which all model setups captured well (Figure B9). During November, diurnal SO₂ patterns were not captured well (Figure 5; left), although biases are not very large (Figure 5; right), being less than 10 ppb at most sites. At Secunda*, not only are hourly average biases larger than 10 ppb on occasion, but there are some significant differences between schemes, with MYJ and MYNN producing significantly larger biases than the non-local schemes. These large differences in biases are visible during the early morning and late afternoon. From 09 to 16 LT, biases are similarly low for all schemes.

Figure B10 shows time series plots at all sites for November. It is interesting to note that observed concentrations for the first half of the month at Secunda, from 3 to 15 November, are consistently very low, varying only between 2.5 and 4.5 ppb (average = 3 ppb). After 15 November, SO₂ concentrations varied between 0.2 and 113.13 ppb (average = 5.10 ppb) for the remainder of the month. Since having no hourly SO₂ concentrations or peaks higher than 4.5 ppb at a site like Secunda is very unlikely, this could indicate a possible SO₂ instrument fault during the first part of November. At Witbank, some elevated baseline concentrations were observed during the second part of the month, from 9 to 18 November, after no observational data were available for the first part of the month, from 1 to 8 November. On average, correlations between observed and simulated concentrations are higher after Day 18 than before.

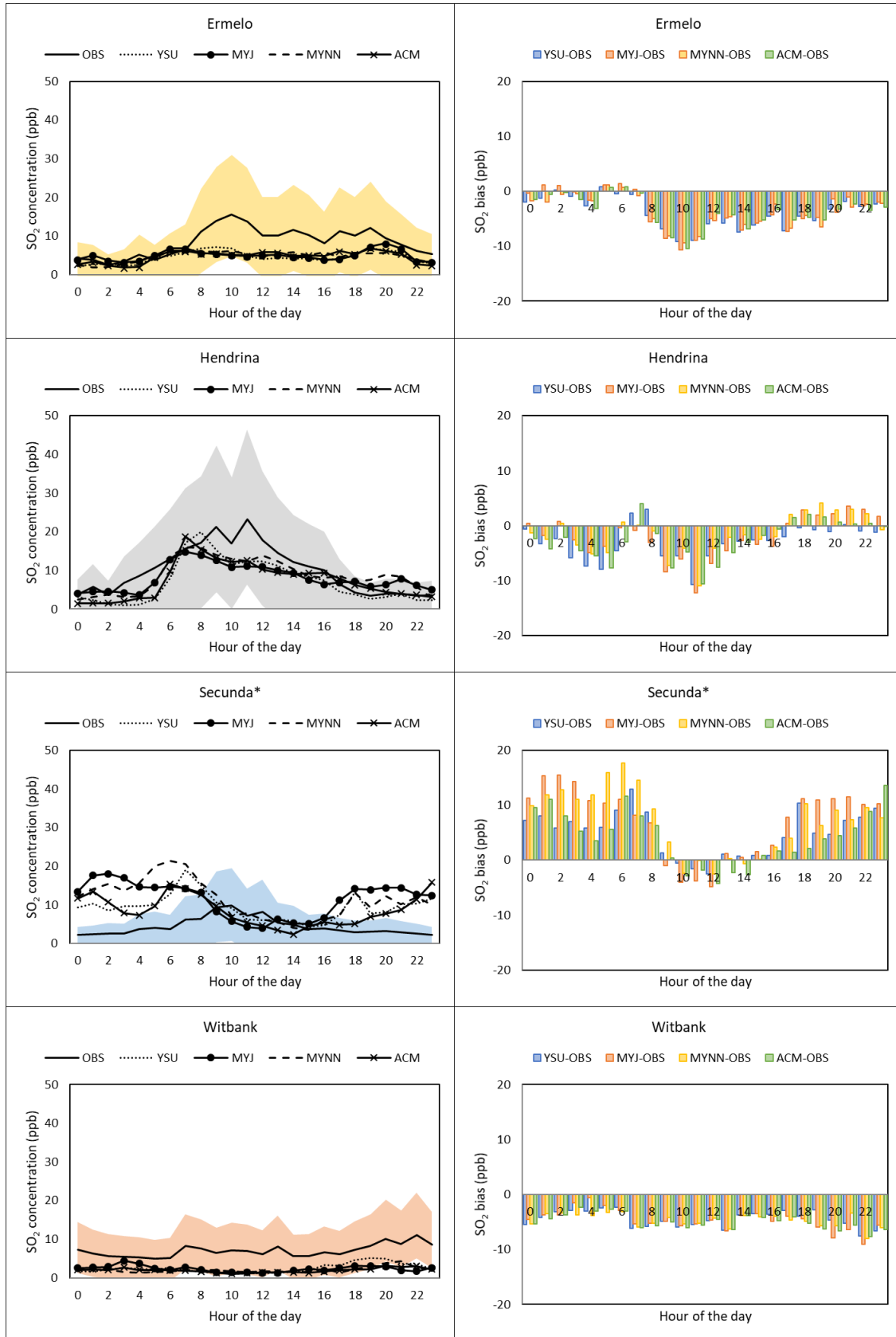


Figure 5. Average hourly SO₂ observed and simulated concentrations for each of the sites (left), and average hourly bias during November (right). The average standard deviation from the observed values is shaded on the diurnal variation plots. An asterisk (*) indicates sites with anomalous data.

4.5.1 SO₂ mid-morning concentration peaks

Of the South African criteria pollutants, SO₂ and NO₂ are major pollutants from industrial tall stacks. Mid-morning concentration peaks, which would align to tall stack emissions, are visible in the diurnal variation of SO₂ (figures 6 and 7). Therefore, simulated SO₂ concentrations are considered to see the effect of the PBL schemes on the transportation of pollution from stacks.

The directional distribution of plumes is influenced by wind direction, and the vertical diffusion is affected by atmospheric stability. Therefore, the choice of PBL schemes will have an effect on ground-level SO₂ concentrations that originated from tall stacks. The magnitudes of the differences in this daytime peak are considered as simulated by the different PBL schemes. PBL heights in this region peaked at differing times during June and November 2016. Periods during which observed and simulated mid-morning SO₂ peaks across sites could be identified were chosen for further analysis. The mid-morning SO₂ peaks were visible from approximately 07 to 12 LT during June 2016, and between 06 and 11 LT during November 2016. These time slices were used to calculate the percentage difference between ground-level SO₂ concentrations simulated by the different schemes.

In order to ease the interpretation of the percentage difference figures, the YSU vs MYNN percentage difference map for June is presented together with the separate average SO₂ concentration maps that comprises it (Figure C1). The YSU vs MYNN percentage difference is derived by taking SO₂ concentrations simulated by CAMx, driven by WRF-ARW output, using YSU minus concentrations from MYNN. Negative percentages mean that the SO₂ concentration simulated by MYNN were larger than those simulated by YSU, while positives mean that YSU-simulated concentrations were larger than those simulated by MYNN. Large negative percentage differences near most of the tall stack sources indicate larger MYNN-simulated concentrations for those areas. In these regions (displayed in dark blue), MYNN simulated plumes, whereas YSU did not. The opposite is true for the regions where positive differences are found (displayed in orange and red on the map), where YSU simulated SO₂ plumes. The remainder of the region did not display large differences between the two schemes (displayed in yellow or light green/blue). The remainder of the plots were interpreted in the same manner.

It is interesting to note in the MYNN plots (MYNN vs YSU/MYJ/ACM) that most of these plot areas show positive percentage differences, meaning that MYNN simulates SO₂ concentrations to be higher than the other schemes during the time of day that a mid-morning SO₂ peak would be expected during June

(Figure 6). This is due to both plume placement and general surface-level emission impacts, i.e. even for lower-level sources, MYNN tends to enhance surface concentrations more than the other schemes. While the majority of the plot shows positive differences, there are some areas near the tall stacks that show negative differences. Here, the other schemes simulate SO₂ plumes, meaning that these schemes simulate SO₂ mixing towards ground level more than MYNN for those specific areas. As expected, the reverse plots (YSU vs MYNN; MYJ vs MYNN; and ACM vs MYNN) are predominantly blue, indicating negative differences in concentrations.

When considering simulated percentage differences during November (Figure C2), plumes are more distinct because, on average, PBL heights are higher during spring. This means that there is a higher chance of SO₂ plumes being mixed towards the surface. Larger positive (dark orange) and negative (dark blue) differences are thus found in Figure C2. These large differences near the significant sources of SO₂ emphasise the spatial sensitivity of the mixing of tall stack SO₂ emissions to PBL schemes. MYNN plots (MYNN vs YSU/MYJ/ACM) during November showed mainly positive percentage differences (except for some significant plumes that were not placed similar to other schemes). This means that MYNN often produced higher concentrations of SO₂ during this time of day.

Kim *et al.* (2015) also found that MYNN produced higher surface concentrations than another scheme (YSU) and attributed this to weaker vertical mixing in MYNN.

While differences between simulated average SO₂ concentrations at the considered monitoring site locations are large at times (e.g. figures 6 and 7; left), percentage SO₂ difference between schemes, seen spatially, during mid-morning hours, vary on average between lows of 0.28% and highs of 20.33%. Compared to the differences displayed near tall stacks (figures 9 and C2), the average percentage differences at the monitoring sites are generally low.

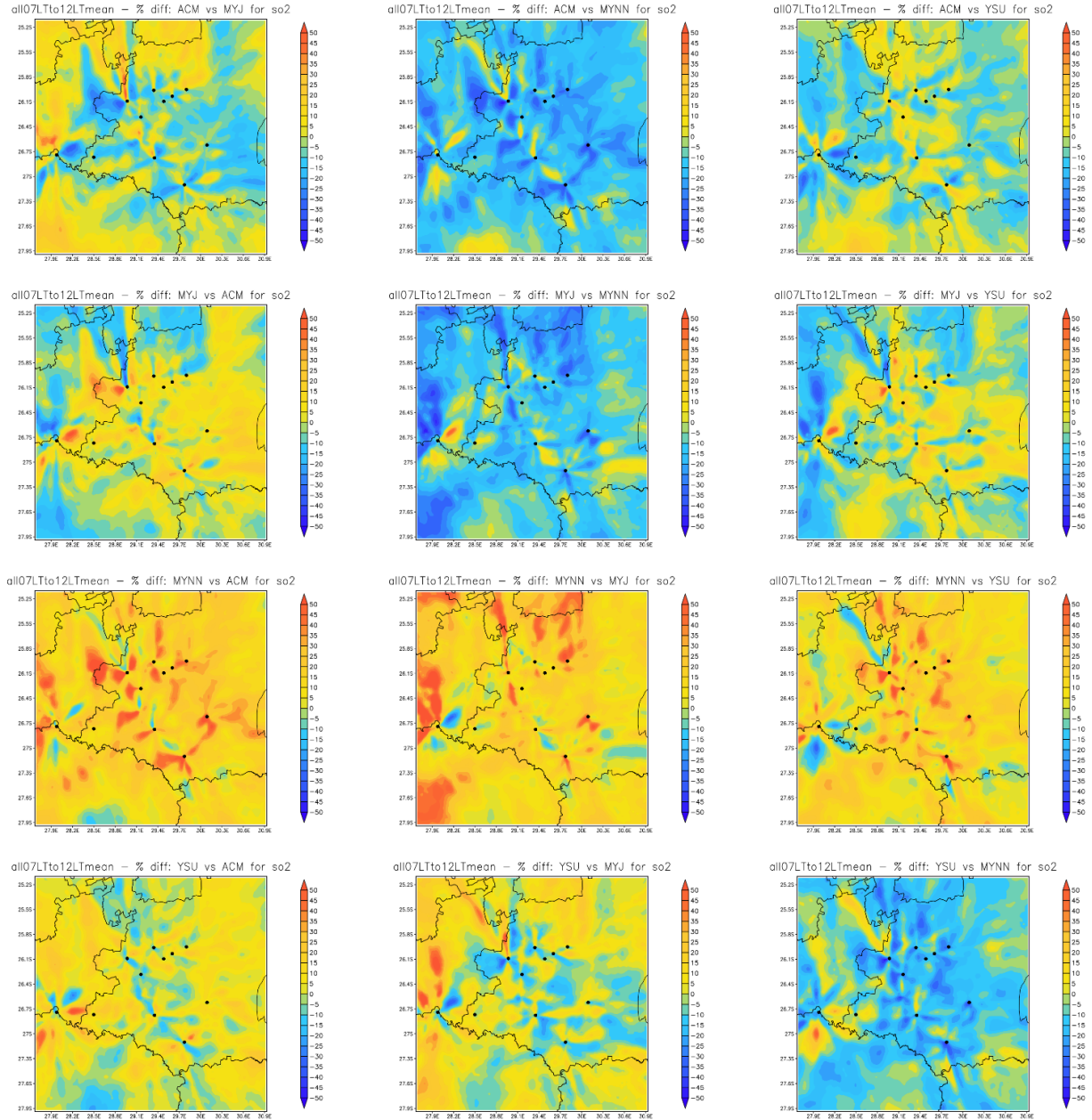


Figure 6. Average percentage difference in simulated ground-level SO₂ concentration from 07 to 12 LT for different scheme combinations during June. Tall stacks from power-generating facilities are indicated with black circles.

5. Discussion

While some research has been conducted on NWP model configurations and their effect on air quality simulations internationally, this influence has not yet been investigated for South Africa. Therefore, there is a need to investigate the sensitivity of different PBL schemes on the simulation of pollutant concentrations in South Africa, particularly in areas with high pollution concentrations, such as in an air pollution priority area. The priority area was selected as the region of interest because of the significant air

pollution challenges it is facing. It is important to gain a better understanding of air pollutant modelling and simulation in these regions, as they are important in terms of air quality policy.

Identifying a single scheme that performs the best across all sites and pollutants is not a realistic expectation for this type of study where multiple sites and types of pollutants are considered. The performance of PBL schemes in air quality model application can depend on pollutant, as in Banks and Baldasano (2016), where the WRF-ARW model was used together with the Community Multiscale Air Quality (CMAQ) modelling system. They conducted a similar sensitivity experiment for O₃, NO₂ and PM₁₀ in Catalonia, Spain. Performance statistics showed that the local BouLac scheme produced a low mean bias for NO₂, while the non-local ACM 2 scheme performed well for O₃. A similar conclusion was made in the present study, where results were very much site and pollutant dependant. On occasion, when considering averages of performance statistics, a best-performing scheme across all sites could be identified. For instance, while ACM only featured as the best-performing scheme a few times, YSU featured as the best-performing scheme most often during November. No single PBL scheme consistently performs well across all sites and pollutants, but the two local schemes (MYJ and MYNN) often performed well across pollutants.

The differences between the simulations and average statistics produced by the different schemes were predominantly small, but the best-performing schemes could, in most cases, be identified when calculating averages across sites. While the considered schemes perform similarly on a diurnal scale (e.g. O₃ during June and November), some differences were noticed between schemes for the other pollutants (e.g. NO₂ during June and November, and PM_{2.5} and PM₁₀ during November).

The reproduction of pollutant concentrations depends on the processes within the air quality model, meteorological inputs from the NWP model, as well as the emission inventory. Therefore, a possible source of uncertainty associated with the type of research presented here is from the emissions.

The under-estimation, over-estimation or omission of certain emission sources can contribute to erroneous simulations. For instance, in the case of Banks and Baldasano (2016), surface PM₁₀ was shown to be the worst performer of all the air quality variables evaluated, with low correlations between the CMAQ model and observations. However, they stated that a possible source of the uncertainty could be the emissions inventory model used (the High Elective Resolution Modelling Emission System (HERMES)). In another instance, the

under-estimation of PM₁₀ concentrations was linked to uncertainties in PM₁₀ emissions, in particular, road dust re-suspension, combined with an over-estimation of vertical mixing at high altitudes at night (Kim *et al.*, 2015).

Another important source of uncertainty is the reproduction of meteorological variables like PBL height. Long-range pollutants, emitted at ground level, like SO₂, PM₁₀, and PM_{2.5}, are strongly influenced by the variation of the PBL. De Lange *et al.* (2021) previously conducted a study focused on meteorological variables across the same region. The results indicated that different PBL schemes perform well, simulating different variables, especially during June. It was ultimately recommended that a local scheme, which uses the TKE method, be used to simulate meteorology for the Highveld region during winter. These schemes better represent stable conditions as the coupling of vertical atmospheric layers is not as enhanced as in spring. During spring, MYJ is clearly the preferred scheme for simulating meteorology for the Highveld. For air quality simulations, no single PBL scheme consistently performs well across all sites and pollutants, but the two local schemes (MYJ and MYNN) often performed well.

In terms of the spatial distribution of simulated ground-level mid-morning concentrations of SO₂, a large sensitivity to the PBL scheme used exists, compared to what is seen in the monitoring station location data. This could be because of MYNN's low PBL height threshold ($1.0 \times 10^{-6} \text{ m}^2\text{s}^{-2}$), as described in Table 1. This low PBL height threshold translates to the PBL being simulated at a lower level in the atmosphere, when compared to the other TKE method scheme (MYJ). Weaker vertical mixing associated with MYNN has previously also been identified as a reason for this scheme producing higher surface concentrations of PM₁₀, PM_{2.5} and NO₂ than YSU (Kim *et al.*, 2015).

6. Summary and conclusion

Air quality models have a key role to play in air quality management in South Africa. Thus, their parameterisation and outputs must be investigated to ensure robust results for decision making. An understanding of the sensitivity of pollutant concentrations to PBL schemes in NWP models can provide insight into model results, and possibly advance the accuracy of air pollution modelling. The results from this study should be considered when configuring NWP models for the simulation of air quality in the Highveld region.

Identifying a single PBL scheme that consistently performs best across the five sites (Ermelo, Hendrina, Middelburg, Secunda and Witbank), the two seasons (spring and winter) and five pollutants (NO₂, O₃, PM_{2.5}, PM₁₀ and SO₂) is not a realistic expectation from this type of study. Therefore, this study was focused on the

sensitivity of simulated surface pollution concentrations to WRF-ARW-model PBL schemes. Differences between the simulations and statistics (averages, standard deviations, bias, mean absolute errors and correlations) produced by the schemes were predominantly small, but in most cases, when calculating averages across sites, a best-performing scheme could be identified.

Considering all the results, ACM appeared as the best-performing scheme the least number of times, only featuring when considering O₃ concentrations, and on occasion for SO₂. YSU regularly featured as the best-performing scheme during November for NO, NO₂ and O₃, and less often during June (mostly for O₃). MYNN also regularly appeared as the best-performing scheme, especially in terms of mean absolute error, when considering PM during June and November, and for both periods when considering SO₂. The local scheme, MYJ, often performed well across sites, pollutants (especially NO₂ and PMs) and seasons. No single PBL scheme consistently performed well across all sites and pollutants, but the local schemes featured as the best-performing schemes across all pollutants more regularly than the non-local schemes.

The underlying causes of the variability in performance of the different PBL schemes when simulating pollutant concentrations are diverse. Not only will closure type and how the schemes deal with the variables in the equations of motion (i.e. order of turbulence) in the scheme cause variability, but also the method and threshold used to calculate PBL height. Another key cause of variability between schemes, which was not explicitly demonstrated in this study, can be attributed to surface layer parameterization scheme (or SLS) used.

Nevertheless, what should be considered when configuring the WRF-ARW model are the different schemes that perform well when simulating the different air pollutants. For instance, when conducting research focussed on the simulation of surface-level O₃ for the Highveld region, one should consider using a non-local schemes (YSU or ACM), but when conducting research pertaining to PM pollution, a local scheme (MYJ or MYNN) is best suited.

The investigation of mid-morning SO₂ concentration peaks led to the conclusion that sensitivity exists in the simulation of SO₂ plumes from tall stacks between schemes. Spatially, MYNN often produced higher concentrations of SO₂ than the other schemes. Tall stacks are large sources of emissions in the region, and thus more work is needed to understand the performance of the different schemes in simulating the mixing of SO₂ plumes from tall stacks.

Acknowledgments

The authors acknowledge the South African Department of Environmental Affairs, Forestry and Fisheries, Eskom and the South African Weather Service for the use of their pollutant concentration data. We thank the South African Department of Environmental Affairs, Forestry and Fisheries for the use of its emission inventory, as developed by the CSIR for the Highveld Health Study. Both the WRF-ARW and CAMx, model runs were performed on the computer infrastructure of the Centre for High Performance Computing (CHPC) at the CSIR. Rebecca Garland and Mogesh Naidoo were funded by a CSIR Parliamentary Grant. We would like to thank the CSIR's Centre for High Performance Computing for the provision of computational resources. This work was supported by Sasol through the Laboratory for Atmospheric Studies at the University of Pretoria, as well as the University of Pretoria.

References

- Balashov, N., Thompson, A., Piketh, S. and Langerman, K., 2014. Surface ozone variability and trends over the South African Highveld from 1990 to 2007. *Journal of Geophysical Research: Atmospheres*, 119(7), pp. 4323–4342.
- Banks, R., Tiana-Alsina, J., Rocadenbosch, F. and Baldasano J., 2015. Performance evaluation of the boundary-layer height from Lidar and the Weather Research and Forecasting model at an urban coastal site in the north-east Iberian peninsula. *Boundary-Layer Meteorology*, 157(2), pp. 265–292. <https://doi.org/10.1007/s10546-015-0056-2>.
- Banks, R. and Baldasano, J., 2016. Impact of WRF model PBL schemes on air quality simulations over Catalonia, Spain. *The Science of The Total Environment*, 572, pp. 98–113. <https://doi.org/10.1016/j.scitotenv.2016.07.167>.
- Belelie, M., Burger, R., Mkhathshwa, G. and Piketh, S., 2019. Assessing the impact of Eskom power plant emissions on ambient air quality over KwaZamokuhle. *Clean Air Journal*, 29(1).
- Broxton, P. D., Zeng, X., Sulla-Menashe, D. and Troch, P. A. 2014. A global land cover climatology using MODIS data. *Journal of Applied Meteorology and Climatology*, 53(6), pp. 1593-1605. <https://doi.org/10.1175/JAMC-D-13-0270.1>.
- Cadet, J., Bencherif, H., Portafaix, T., Lamy, K., Ncongwane, K., Coetzee, G. and Wright, C., 2017. Comparison of ground-based and satellite-derived solar UV index levels at six South African sites. *International Journal of Environmental Research and Public Health*, 14(11), p. 1384.
- Cairncross E., Dalvie A., Euripidou R., Irlam J., Naidoo R.N. (2018) Climate Change, Air Pollution and Health in South Africa. In: Akhtar R., Palagiano C. (eds) Climate Change and Air Pollution. Springer Climate. Springer, Cham. https://doi.org/10.1007/978-3-319-61346-8_20.

- Cohen, J., 1988. Statistical power analysis for the behavioral sciences (2nd ed.), Lawrence Erlbaum Associates, New Jersey.
- Cohen, A.E., Cavallo, S.M., Coniglio, M.C. and Brooks, H.E., 2015. A review of planetary boundary layer parameterization schemes and their sensitivity in simulating southeastern US cold season severe weather environments. *Weather Forecasting*, 30, pp. 591–612. <https://doi.org/10.1175/WAF-D-14-00105.1>.
- Collett, K., Piketh, S. and Ross, K., 2010. An assessment of the atmospheric nitrogen budget on the South African highveld. *South African Journal of Science*, 106(5/6).
- Crétat, J., Pohl, B., Richard, Y. and Drobinski, P., 2012. Uncertainties in simulating regional climate of Southern Africa: Sensitivity to physical parameterisations using WRF. *Climate Dynamics*, 38(3–4), pp. 613–634. <https://doi.org/10.1007/s00382-011-1055-8>.
- Cuchiara, G., Li, X., Carvalho, J. and Rappenglück, B., 2014. Intercomparison of planetary boundary layer parameterization and its impacts on surface ozone concentration in the WRF/Chem model for a case study in Houston/Texas. *Atmospheric Environment*, 96, pp. 175–185.
- Department of Environmental Affairs (DEA), 2012. Declaration of the Waterberg Priority Area in terms of the National Environmental Management: Air Quality Act, Act No. 39 of 2004. *Government Gazette*, 35435, 15 June 2012.
- Department of Environmental Affairs (DEA), 2013. The medium term review of the 2009 Vaal Triangle Airshed Priority Area: Air quality management plan final review report. Compiled by Escience Associates Consulted for DEA, June 2013.
- Department of Environmental Affairs (DEA), 2015. The medium-term review of the 2011 Highveld Priority Area (HPA): Air Quality Management Plan. Draft review report, DEA.
- Department of Environmental Affairs and Tourism (DEAT), 2006. Declaration of the Vaal Triangle Air-Shed priority area in terms of section 18 (1) of the National Environmental Management: Air Quality Act, Act No. 39 of 2004. *Government Gazette*, 28732, 21 April 2006.
- Department of Environmental Affairs and Tourism (DEAT), 2007. Declaration of the Highveld as a priority area in terms of section 18 (1) of the National Environmental Management: Air Quality Act, Act No. 39 of 2004. *Government Gazette*, 30518, 23 November 2007.
- De Lange, A., Garland, R. and Dyson, L., 2019. Estimating particulate matter (PM) concentrations from a meteorological index for data-scarce regions: A pilot study. *Atmospheric Pollution Research*, 10(5), pp. 1553–1564. <https://doi.org/10.1016/j.apr.2019.05.004>.
- De Lange, A., Naidoo, M., Garland, R. and Dyson, L., 2021. Sensitivity of meteorological variables on planetary boundary layer parameterisation schemes in the WRF-ARW model. *Atmospheric Research*. <https://doi.org/10.1016/j.atmosres.2020.105214>.
- Dyson, L.L., Van Heerden, J. and Sumner, P.D., 2015. A baseline climatology of sounding-derived parameters associated with heavy rainfall over Gauteng, South Africa. *International Journal of Climatology*, 35, pp. 114–127.
- Emmons, L.K., Walters, S., Hess, P.G., Lamarque, J-F., Pfister, G.G., Fillmore, D., Granier, C., Guenther, A., Kinnison, D., Laepple, T., Orlando, J., Tie, X., Tyndall, G., Wiedinmyer, C., Baughcum, S.L. and Kloster, S.,

2010. Description and evaluation of the model for ozone and related chemical tracers, version 4 (MOZART-4), *Geoscientific Model Development*, 3, pp. 43–67. DOI:10.5194/gmd-3-43-2010.
- ENVIRON, 2016. User's guide, Comprehensive Air Quality Model with Extensions (CAMx), Version 6.30. <http://www.camx.com>.
- Gijben, M., 2012. The lightning climatology of South Africa. *South African Journal of Science*, 108, pp. 44–53.
- Gilliam, R.C., Hogrefe, C. and Rao, S.T., 2006. New methods for evaluating meteorological models used in air quality applications. *Atmospheric Environment*, 40(26), pp. 5073–5086. <https://doi.org/10.1016/j.atmosenv.2006.01.023>.
- Hahmann, A., Lennard, C., Badger, J., Vincent, C., Kelly, M., Volker, P., Argent, B. and Refslund, J., 2015. Mesoscale modeling for the Wind Atlas of South Africa (WASA) project. <https://doi.org/10.13140/RG.2.1.3735.6887>.
- Hersey, S., Garland, R., Crosbie, E., Shingler, T., Sorooshian, A., Piketh, S. and Burger, R., 2015. An overview of regional and local characteristics of aerosols in South Africa using satellite, ground, and modeling data. *Atmospheric Chemistry and Physics*, 15(8), pp. 4259–4278.
- Hong, S., Noh, Y. and Dudhia, J., 2006. A new vertical diffusion package with an explicit treatment of entrainment processes. *Monthly Weather Review*, 134, pp. 2318–2341, <https://doi.org/10.1175/MWR3199.1>.
- Hong, S. and Lim, J., 2006. The WRF single-moment 6-class microphysics scheme (WSM6). *Journal of the Korean Meteorological Society*, 42, pp. 129–151.
- Iacono, M.J., Delamere, J.S. Mlawer, E.J., Shephard, M.W., Clough, S.A., Collins, W.D., 2008. Radiative forcing by long-lived greenhouse gases: Calculations with the AER radiative transfer models. *Journal of Geophysical Research*, 113, D13103. <https://doi.org/10.1029/2008JD009944>.
- Janjić, Z.I., 1994. The Step-Mountain Eta Coordinate Model: Further developments of the convection, viscous sublayer, and turbulence closure schemes. *Monthly Weather Review*, 122, pp. 927–945. [https://doi.org/10.1175/1520-0493\(1994\)122<0927:TSMECM>2.0.CO;2](https://doi.org/10.1175/1520-0493(1994)122<0927:TSMECM>2.0.CO;2).
- Kain, J.S., 2004. The Kain–Fritsch convective parameterization: An update. *Journal of Applied Meteorology*, 43, pp. 170–181. [https://doi.org/10.1175/1520-0450\(2004\)043<0170:TKCPAU>2.0.CO;2](https://doi.org/10.1175/1520-0450(2004)043<0170:TKCPAU>2.0.CO;2).
- Kim, Y., Sartelet, K., Raut, J. and Chazette, P., 2015. Influence of an urban canopy model and PBL schemes on vertical mixing for air quality modeling over Greater Paris. *Atmospheric Environment*, 107, pp. 289–306. <https://doi.org/10.1016/j.atmosenv.2015.02.011>.
- Kong, X., Forkel, R., Sokhi, R.S., Suppan, P., Baklanov, A., Gauss, M., Brunner, D., Barò, R., Balzarini, A., Chemel, C., Curci, G., Jiménez-Guerrero, P., Hirtl, M., Honzak, L., Im, U., Pérez, J.L., Pirovano, G., San Jose, R., Schlünzen, K.H., Tsegas, G., Tuccella, P., Werhahn, J., Žabkar, R. and Galmarin, S., 2015. Analysis of meteorology–chemistry interactions during air pollution episodes using online coupled models within AQMEII phase-2. *Atmospheric Environment*, 115, pp. 527–540. <https://doi.org/10.1016/j.atmosenv.2014.09.020>.
- Lazaridis, M., 2012. *First principles of meteorology and air pollution*, Springer.
- Lerche, C., Philipsen, P. and Wulf, H., 2017. UVR: Sun, lamps, pigmentation and vitamin D. *Photochemical and Photobiological Sciences*, 16(3), pp. 291–301.

- Liao, J., Wang, T., Wang, X., Xie, M., Jiang, Z., Huang, X. and Zhu, J., 2014. Impacts of different urban canopy schemes in WRF/Chem on regional climate and air quality in Yangtze River Delta, China. *Atmospheric Research*, 145–146, pp. 226–243. <https://doi.org/10.1016/j.atmosres.2014.04.005>.
- Lourens, A., Beukes, J., Van Zyl, P., Fourie, G., Burger, J., Pienaar, J., Read, C. and Jordaan, J., 2011. Spatial and temporal assessment of gaseous pollutants in the Highveld of South Africa. *South African Journal of Science*, 107(1/2).
- Nakanishi, M., Niino, H., 2006. An improved Mellor–Yamada Level-3 Model: Its numerical stability and application to a regional prediction of advection fog. *Boundary-Layer Meteorology*, 119, p. 397. <https://doi.org/10.1007/s10546-005-9030-8>.
- Ocak, S. and Turalioglu, S.F., 2008. Effect of meteorology on the atmospheric concentrations of traffic- related pollutants in Erzurum, Turkey. *Journal of International Environmental and Application Science*, 3.
- Pérez, C., Jiménez, P., Jorba, O., Sicard, M. and Baldasano, J. 2006. Influence of the PBL scheme on high-resolution photochemical simulations in an urban coastal area over the Western Mediterranean. *Atmospheric Environment*, 40(27), pp. 5274–5297.
- Pleim, J.E., 2007. A combined local and nonlocal closure model for the atmospheric boundary layer. Part I: Model description and testing. *Journal of Applied Meteorology and Climatology*, 46, pp. 1383–1395. <https://doi.org/10.1175/JAM2539.1>.
- Pohl, B., Rouault, M. and Roy, S.S., 2014. Simulation of the annual and diurnal cycles of rainfall over South Africa by a regional climate model. *Climate Dynamics*, 43(7–8), pp. 2207–2226. <https://doi.org/10.1007/s00382-013-2046-8>.
- Pretorius, I., 2015. Impacts and control of coal-fired power station emissions in South Africa. PhD thesis, Department of Geography and Environmental Management, North West University.
- Radaideh, J.A., 2017. Effect of meteorological variables on air pollutants variation in arid climates. *Journal of Environmental and Analytical Toxicology*, 7, p. 478. <https://doi.org/10.4172/2161-0525.1000478>.
- Ratna, S.B., Ratnam, J.V., Behera, S.K., Rautenbach, C.J., Ndarana, T., Takashi, K. and Yamagata, T., 2014. Performance assessment of three convective parameterization schemes in WRF for downscaling summer rainfall over South Africa. *Climate Dynamics*, 42(11–12), pp. 2931–2953. <https://doi.org/10.1007/s00382-013-1918-2>.
- Ritter, M., Müller, M.D., Jorba, O., Parlow, E., Liu, L-J.S., 2013. Impact of chemical and meteorological boundary and initial conditions on air quality modeling: WRF-Chem sensitivity evaluation for a European domain. *Meteorology and Atmospheric Physics*, 119, pp. 59–70. <https://doi.org/10.1007/s00703-012-0222-8>.
- Rogers, R.E., Deng, A., Stauffer, D.R., Gaudet, B.J., Jia, Y., Soong, S. and Tanrikulu, S., 2013. Application of the weather research and forecasting model for air quality modeling in the San Francisco bay area. *Journal of Applied Meteorology and Climatology*, 52, pp. 1953–1973. <https://doi.org/10.1175/JAMC-D-12-0280.1>.
- Saha, S., Moorthi, S., Wu, X., Wang, J., Nadiga, S., Tripp, P., Behringer, D., Hou, Y., Chuang, H., Iredell, M., Ek, M., Meng, J., Yang, R., Mendez, M. P., Van den Dool, H., Zhang, Q., Wang, W., Chen, M. and Becker, E., 2011. NCEP Climate Forecast System Version 2 (CFSv2) 6-hourly products. Research Data Archive at

- the National Center for Atmospheric Research, Computational and Information Systems Laboratory.
<https://doi.org/10.5065/D61C1TXF>.
- Skamarock, W.C., Klemp, J.B., Dudhia, J.D., Gill, O., Barker, D.M., Duda, M.G., Huang, X-Y., Wang, W., Powers, J.G., 2008. A description of the advanced research WRF Version 3.
<https://doi.org/10.5065/D68S4MVH>.
- Swap, R., Annegarn, H., Suttles, J., King, M., Platnick, S., Privette, J. and Scholes, R., 2003. Africa burning: A thematic analysis of the Southern African Regional Science Initiative (SAFARI 2000). *Journal of Geophysical Research: Atmospheres*, 108(D13).
- Taljaard, J., 1995. Atmospheric circulation systems, synoptic climatology and weather phenomena of South Africa. Part 2: Atmospheric circulation systems in the South African region. South African Weather Bureau Technical Paper No. 28.
- Tao, Z., Santanello, J.A., Chin, M., Zhou, S., Tan, Q., Kemp, E.M. and Peters-Lidard, C.D., 2013. Effect of land cover on atmospheric processes and air quality over the continental United States – a NASA Unified WRF (NU-WRF) model study. *Atmospheric Chemistry and Physics*, 13, pp. 6207–6226.
<https://doi.org/10.5194/acp-13-6207-2013>.
- Tewari, M., Chen, F., Wang, W., Dudhia, J., LeMone, M. A., Mitchell, K., Ek, M., Gayno, G., Wegiel, J., Cuenca, R.H., 2004. Implementation and verification of the unified NOAA land surface model in the WRF model. 20th conference on weather analysis and forecasting/16th conference on numerical weather prediction.
- Tyson, P.D., Kruger, F.J. and Louw, C.W. (eds.), 1988. Atmospheric pollution and its implications in the eastern Transvaal highveld. South African National Scientific Programmes Report No. 150, Council for Scientific and Industrial Research, Pretoria.
- United States Environmental Protection Agency (US EPA), 2017. QA handbook for air pollution measurement systems: Volume II: Ambient air quality monitoring program. EPA-454/B-17-001.
- United States Government Accountability Office (US GAO), 2011. Information on tall smokestacks and their contribution to interstate transport of air pollution. AIR QUALITY, Washington.
- Venter, A., Vakkar, V., Beukes, J., Van Zyl, P., Laakso, H., Mabaso, D., Tiitta, P., Josipovic, M., Kulmala, M., Pienaar, J. and Laakso, L., 2012. An air quality assessment in the industrialised western Bushveld Igneous Complex, South Africa. *South African Journal of Science*, 108(9/10).
- Wang, J., Zhang, B., Zhang, H. and Lv, M., 2019. The impacts of three PBL schemes on the simulation of boundary layer meteorological factors and air pollutants in Northern China. *IOP Conference Series: Earth and Environmental Science*, 227, p. 052011.
- Yarwood, G., Rao, S., Yocke, M. and Whitten, G.Z., 2005. Updates to the carbon bond chemical mechanism: CB05. Final Report prepared for US EPA.
http://www.camx.com/publ/pdfs/CB05_Final_Report_120805.pdf.
- Zahumensky, I., 2004. Guidelines on quality control procedures for data from automatic weather stations. WMO-No. 955. Geneva, Switzerland.
- Zhang, N., Chen, Y., Gao, H. and Luo, L. 2019. Influence of urban land cover data uncertainties on the numerical simulations of urbanization effects in the 2013 high-temperature episode in Eastern China.

Theoretical and Applied Climatology, 138, pp. 1715–1734. <https://doi.org/10.1007/s00704-019-02926-5>.

Appendix A: Diurnal variation and bias plots

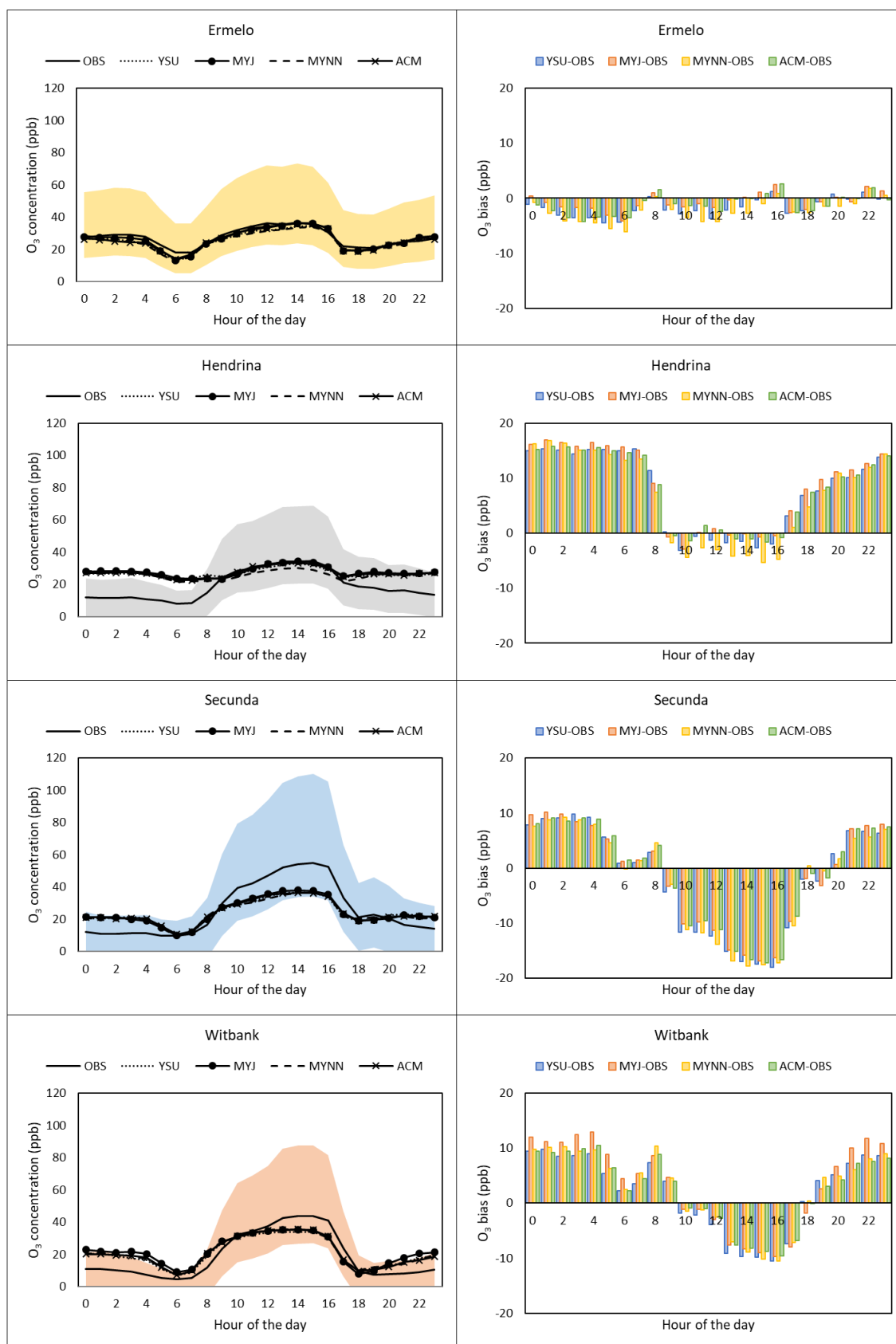


Figure A1. Average hourly O₃ observed and simulated concentration for each of the sites (left), and average hourly bias during June (right). Average SD from observed values is shaded on the diurnal variation plots.

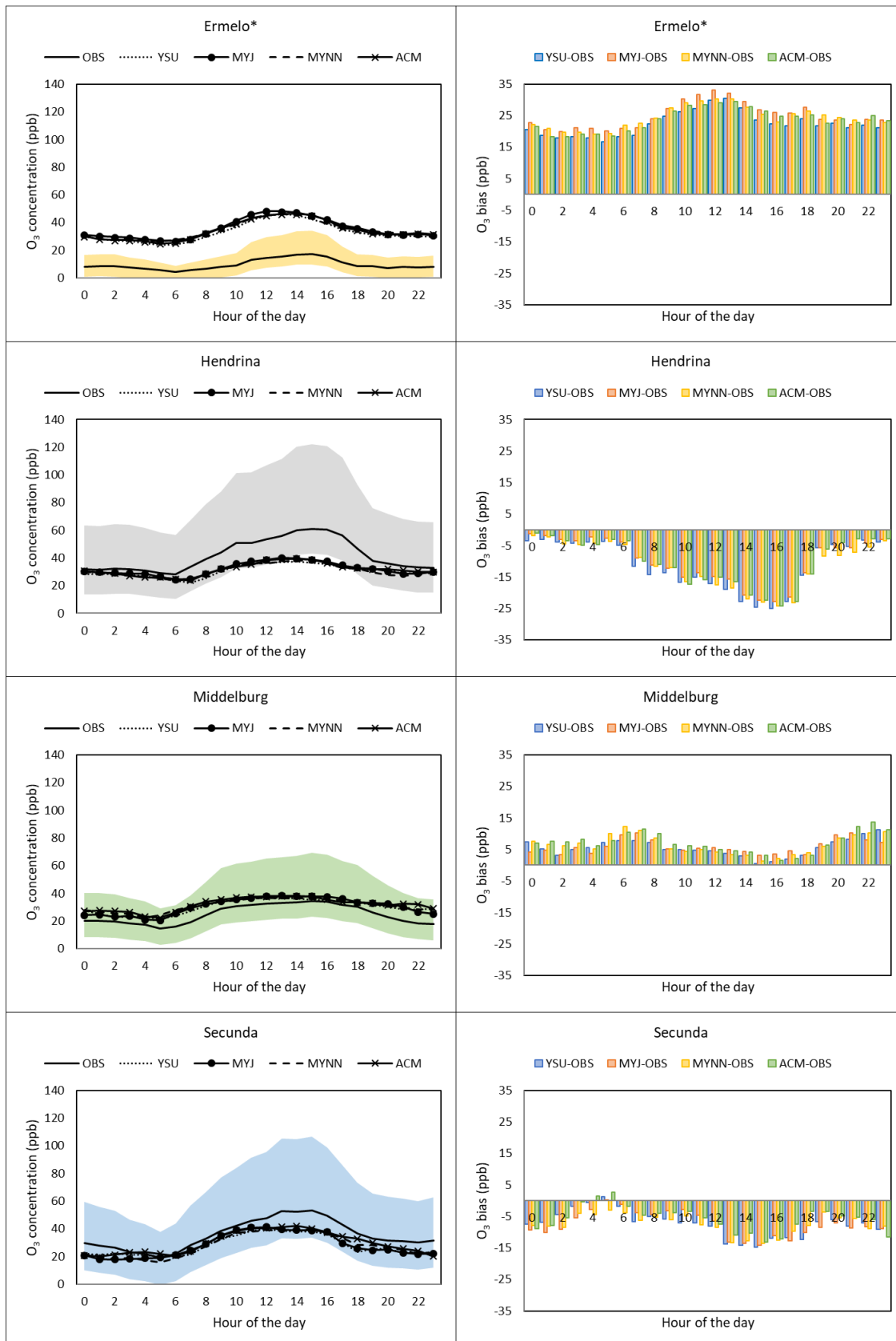


Figure A2. Average hourly O₃ observed and simulated concentration for each of the sites (left), and average hourly bias during November (right). Average SD from observed values is shaded on the diurnal variation plots. An asterisk (*) indicates sites with anomalous data.

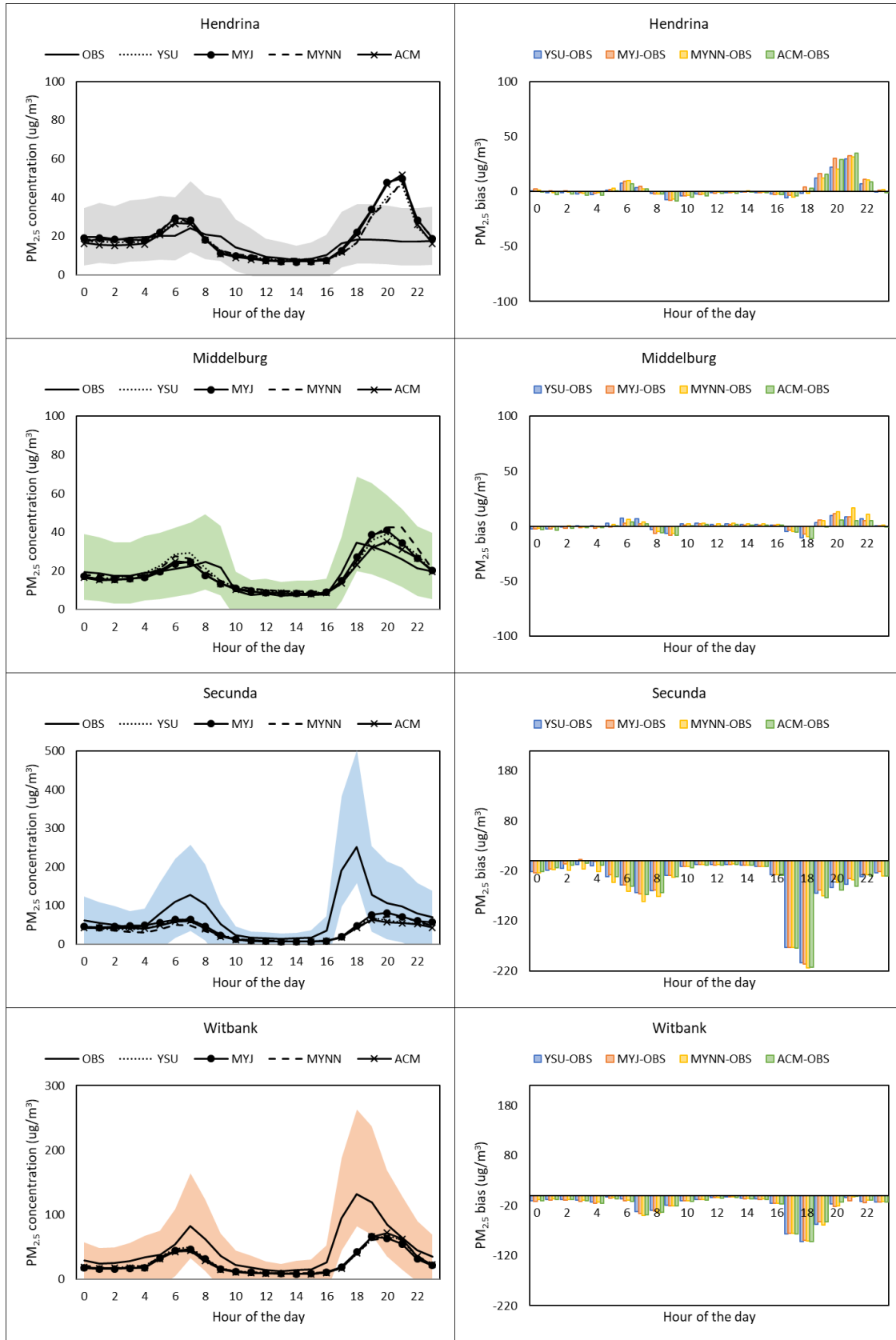


Figure A3. Average hourly $PM_{2.5}$ observed and simulated concentration for each of the sites (left), and average hourly bias during June (right). Average SD from observed values is shaded on the diurnal variation plots.

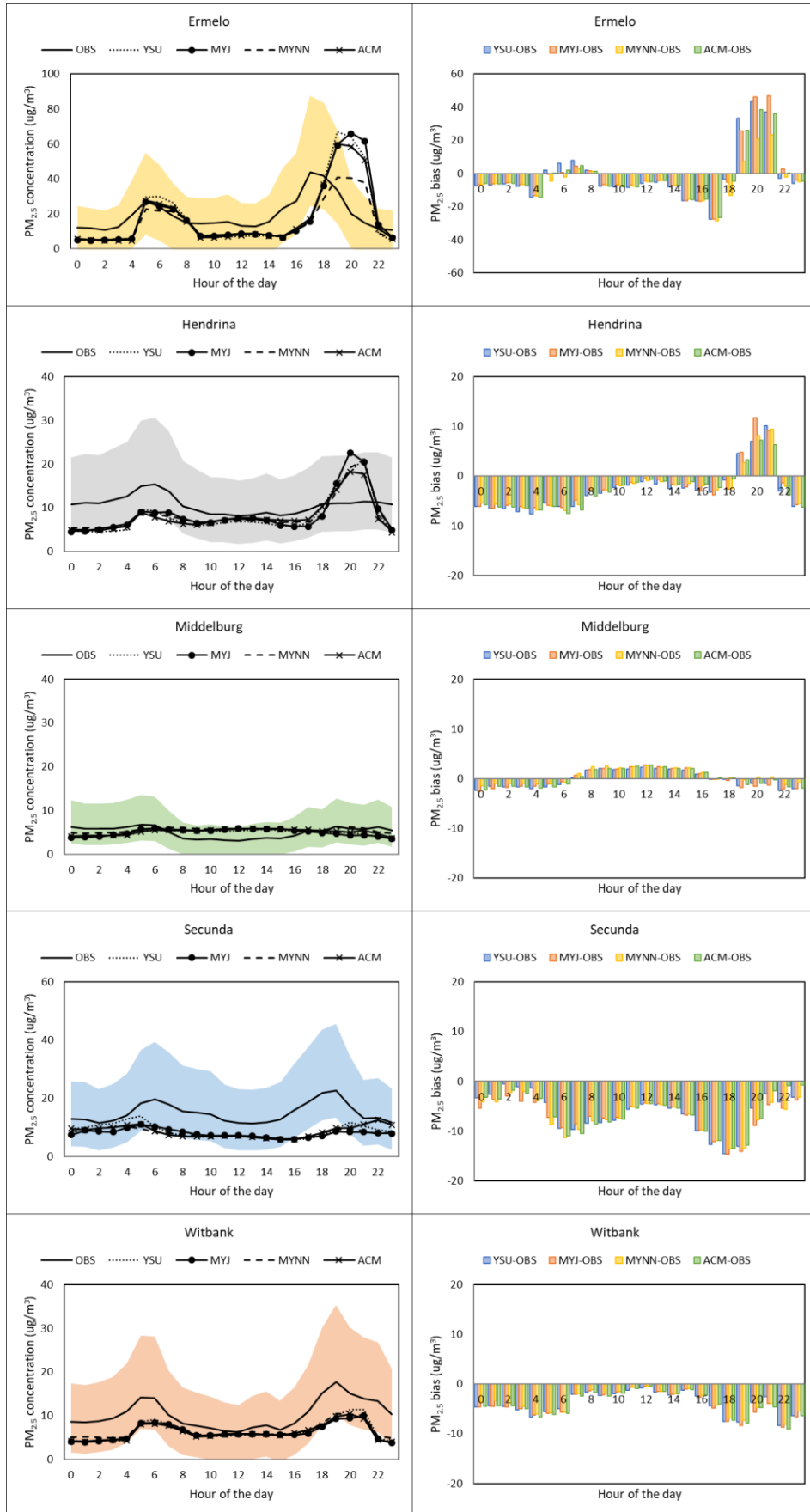


Figure A4. Average hourly $PM_{2.5}$ observed and simulated concentration for each of the sites (left), and average hourly bias during November (right). Average SD from observed values is shaded on the diurnal variation plots.

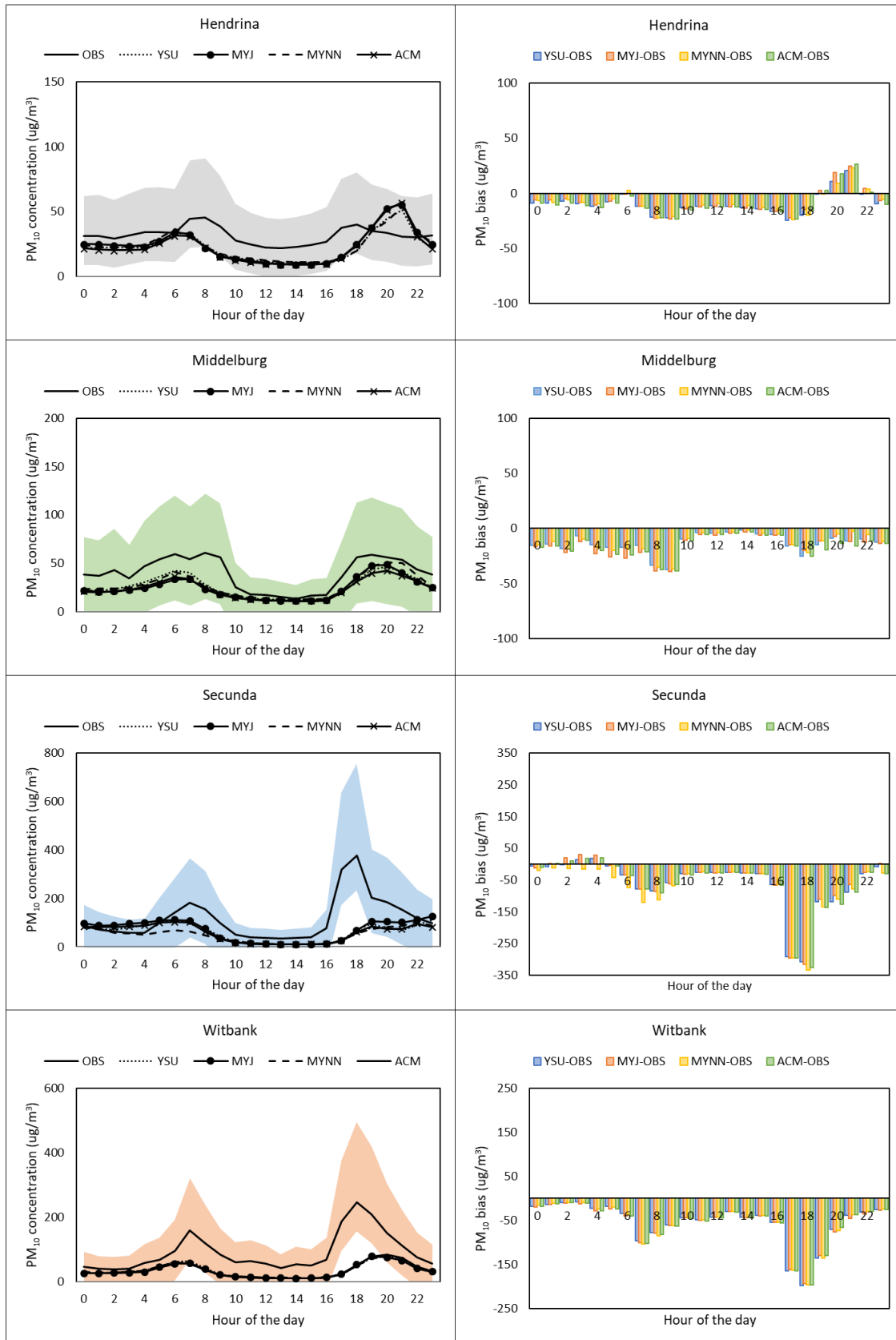


Figure A5. Average hourly PM₁₀ observed and simulated concentration for each of the sites (left), and average hourly bias during June (right). Average SD from observed values is shaded on the diurnal variation plots.

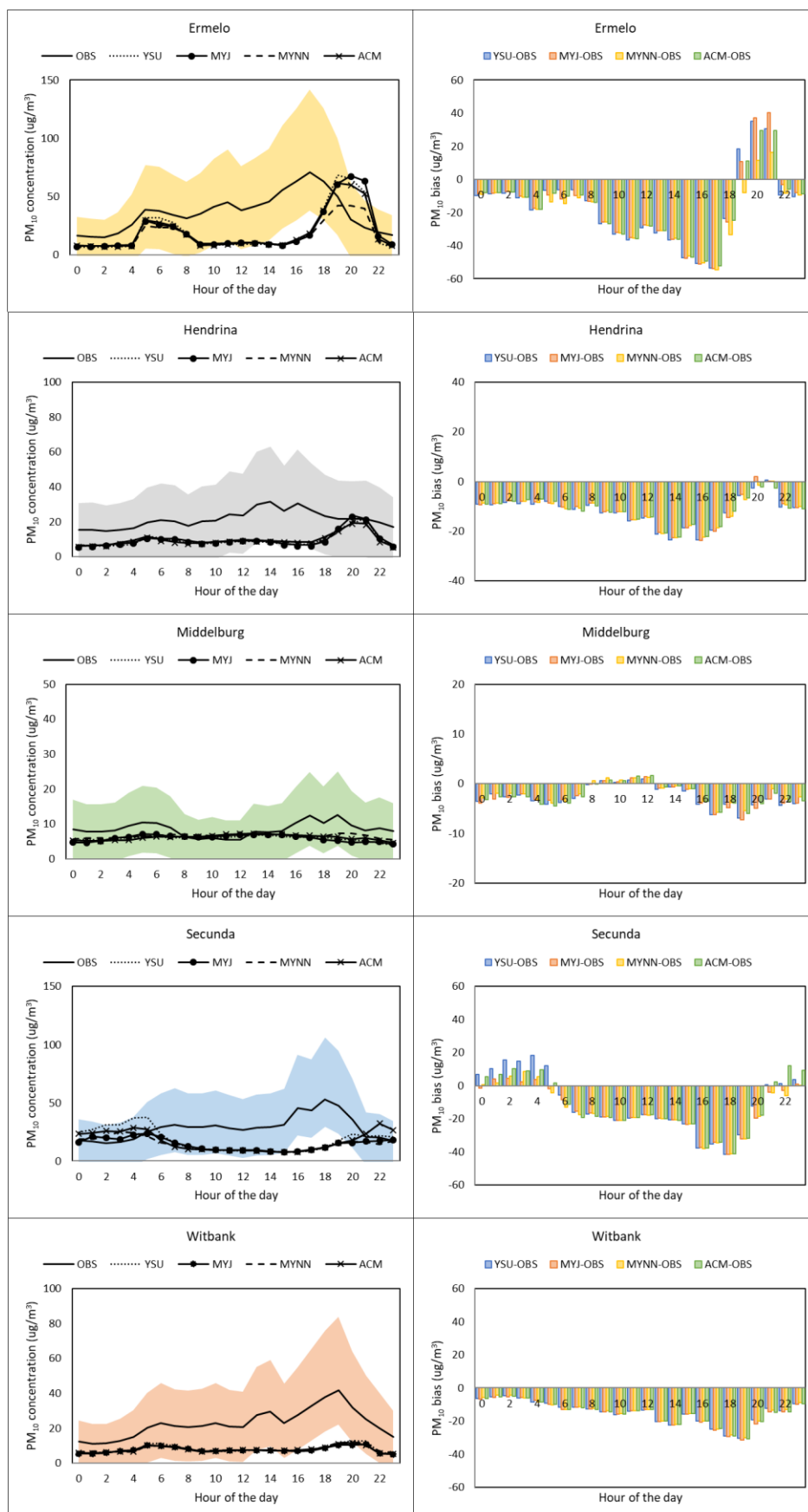


Figure A6. Average hourly PM₁₀ observed and simulated concentration for each of the sites (left), and average hourly bias during November (right). Average SD from observed values is shaded on the diurnal variation plots.

Appendix B: Time series plots

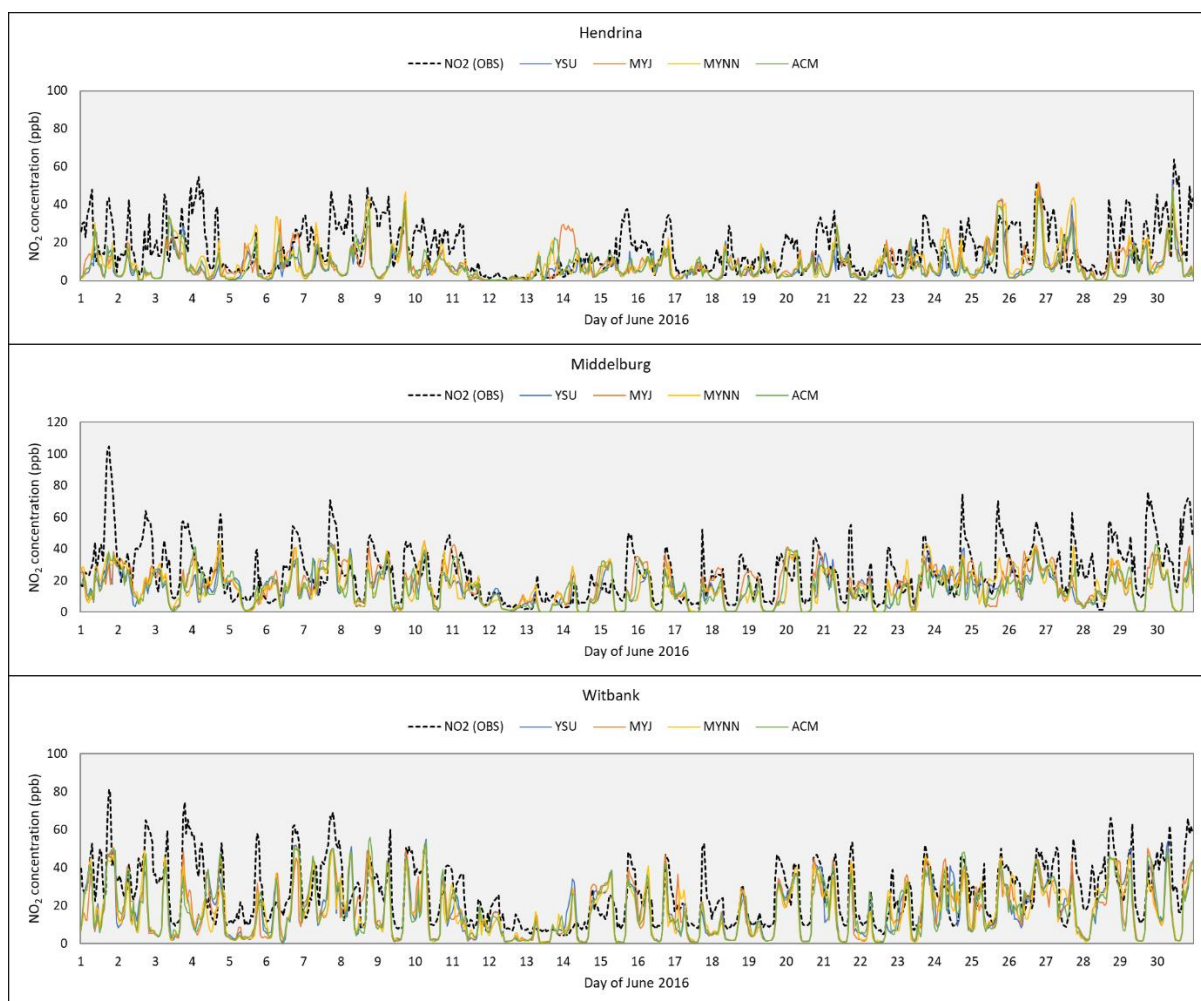


Figure B1. Hourly time series of observed and simulated NO₂ concentrations for June.

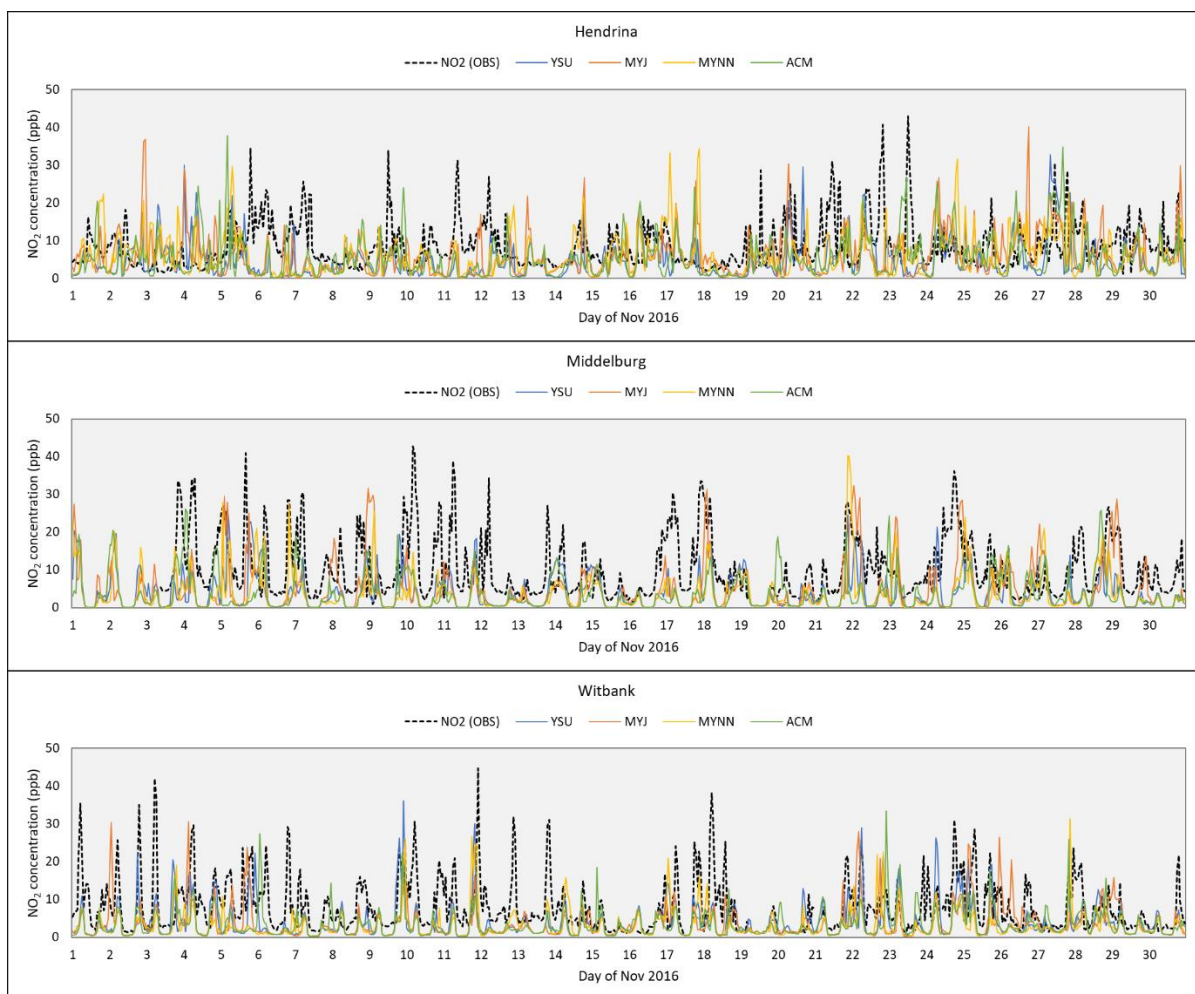


Figure B2. Hourly time series of observed and simulated NO_2 concentrations for November.

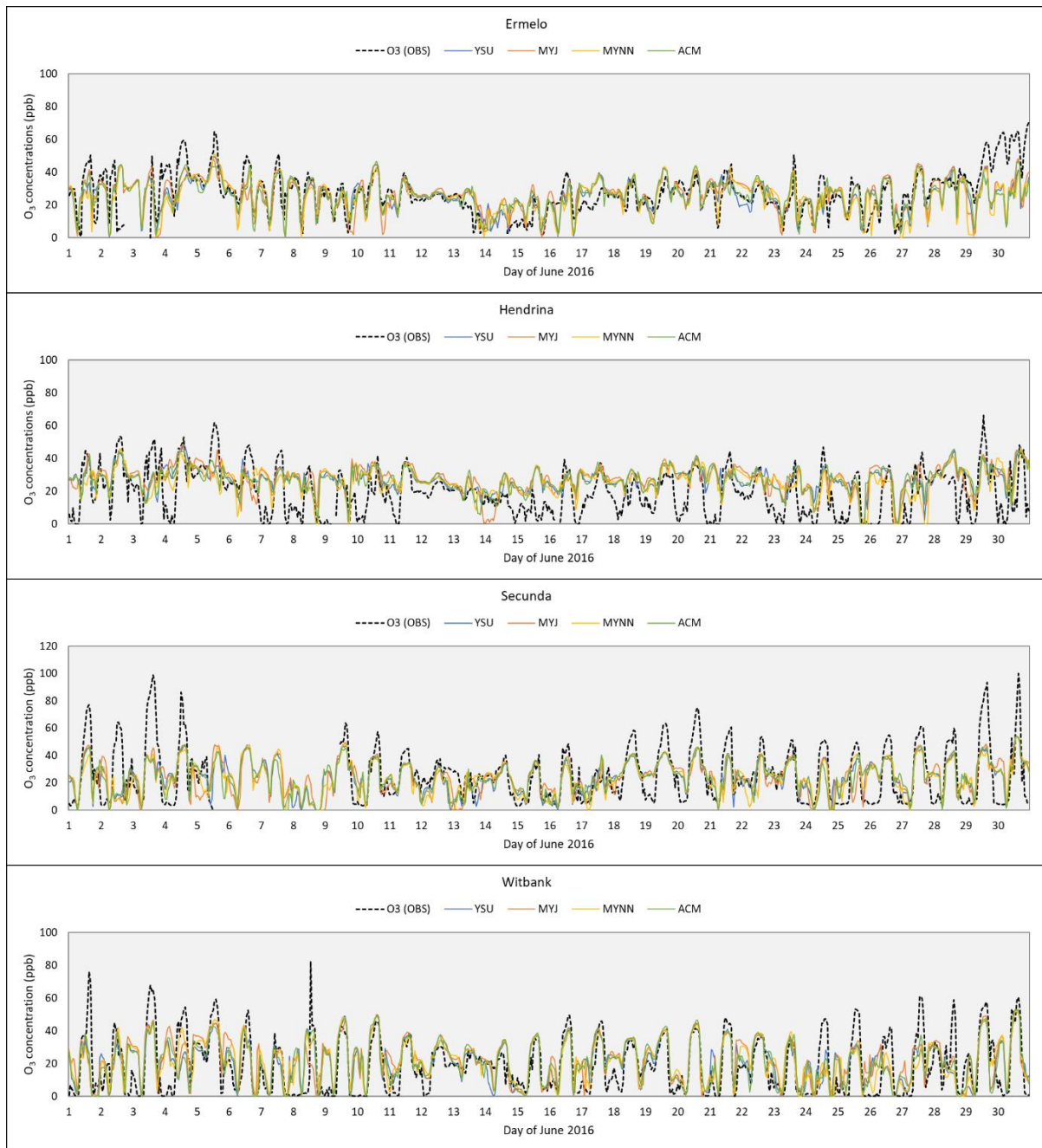


Figure B3. Hourly time series of observed and simulated O₃ concentrations for June.

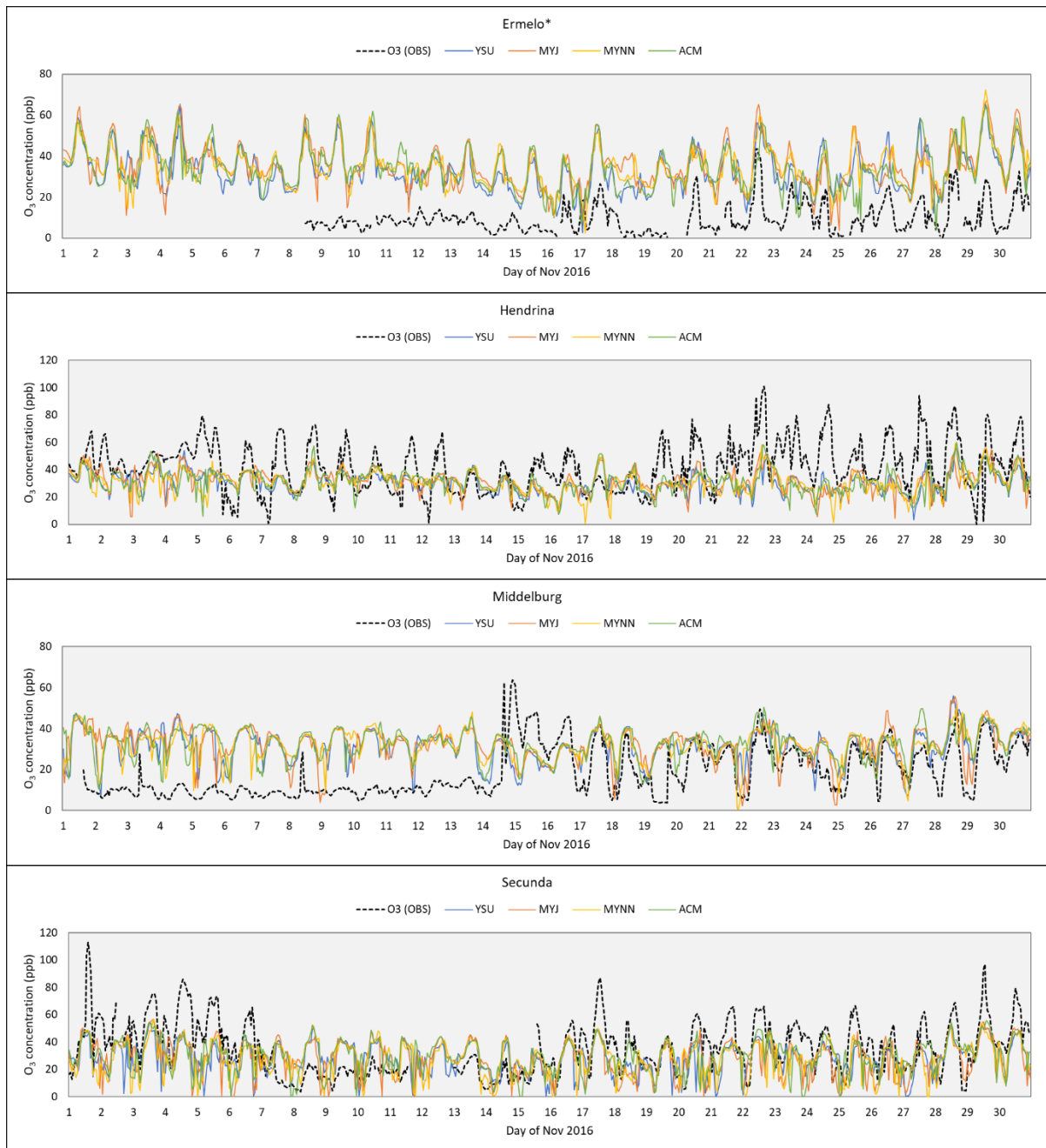


Figure B4. Hourly time series of observed and simulated O₃ concentrations for November. An asterisk (*) indicates sites with anomalous data.

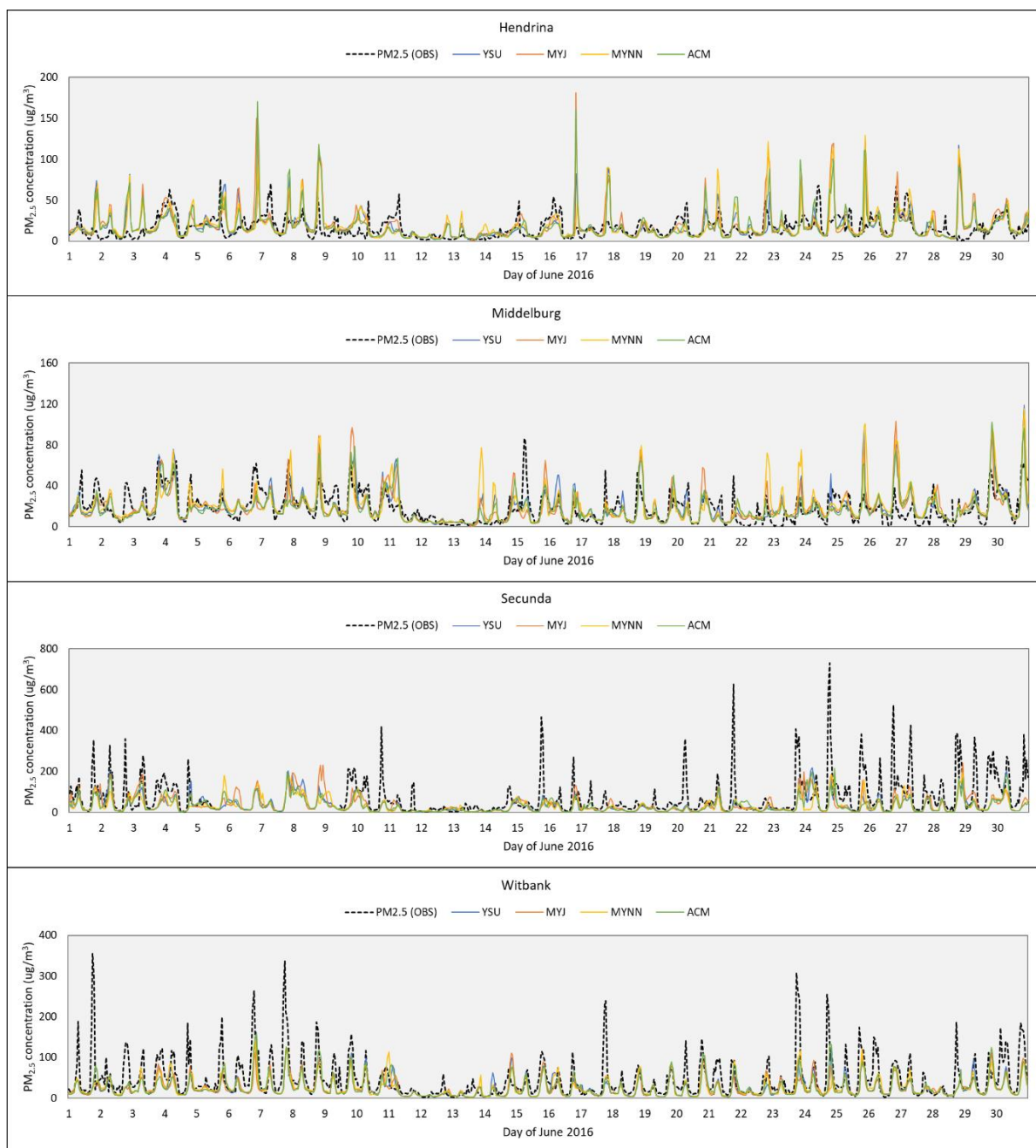


Figure B5. Hourly time series of observed and simulated PM_{2.5} concentrations for June.



Figure B6. Hourly time series of observed and simulated PM_{2.5} concentrations for November.

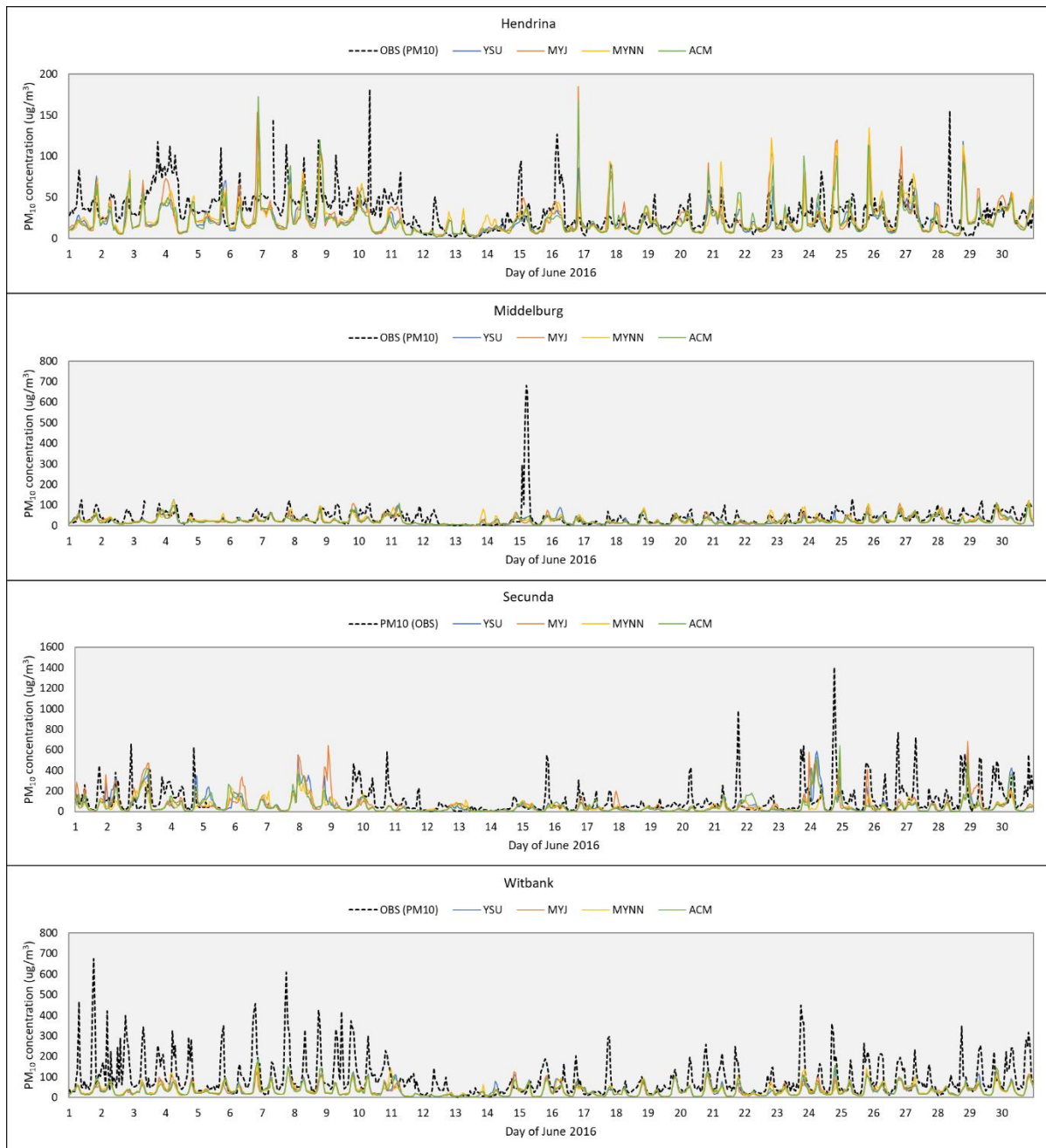


Figure B7. Hourly time series of observed and simulated PM₁₀ concentrations for June.



Figure B8. Hourly time series of observed and simulated PM₁₀ concentrations for November.

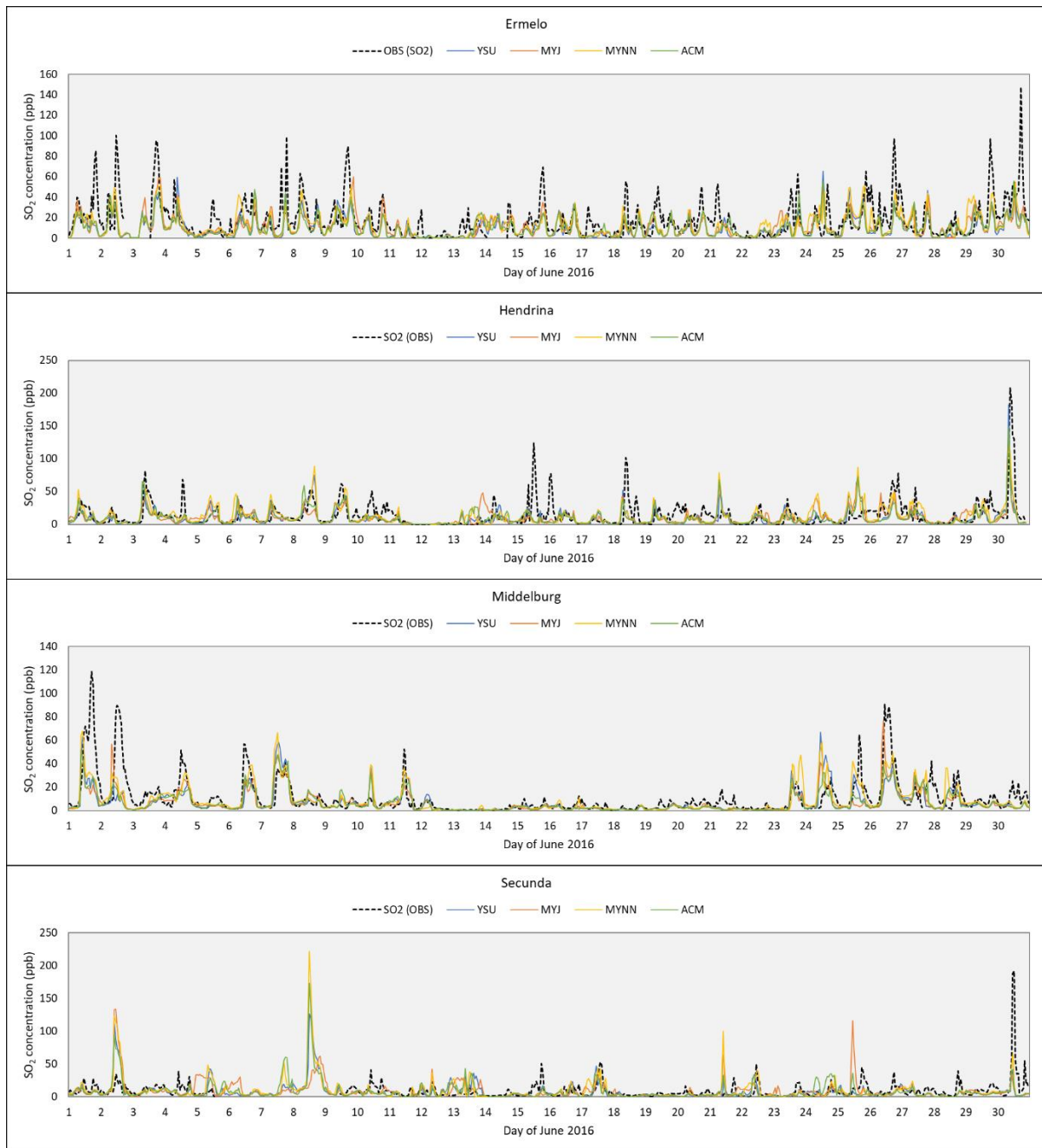


Figure B9. Hourly time series of observed and simulated SO₂ concentrations for June.

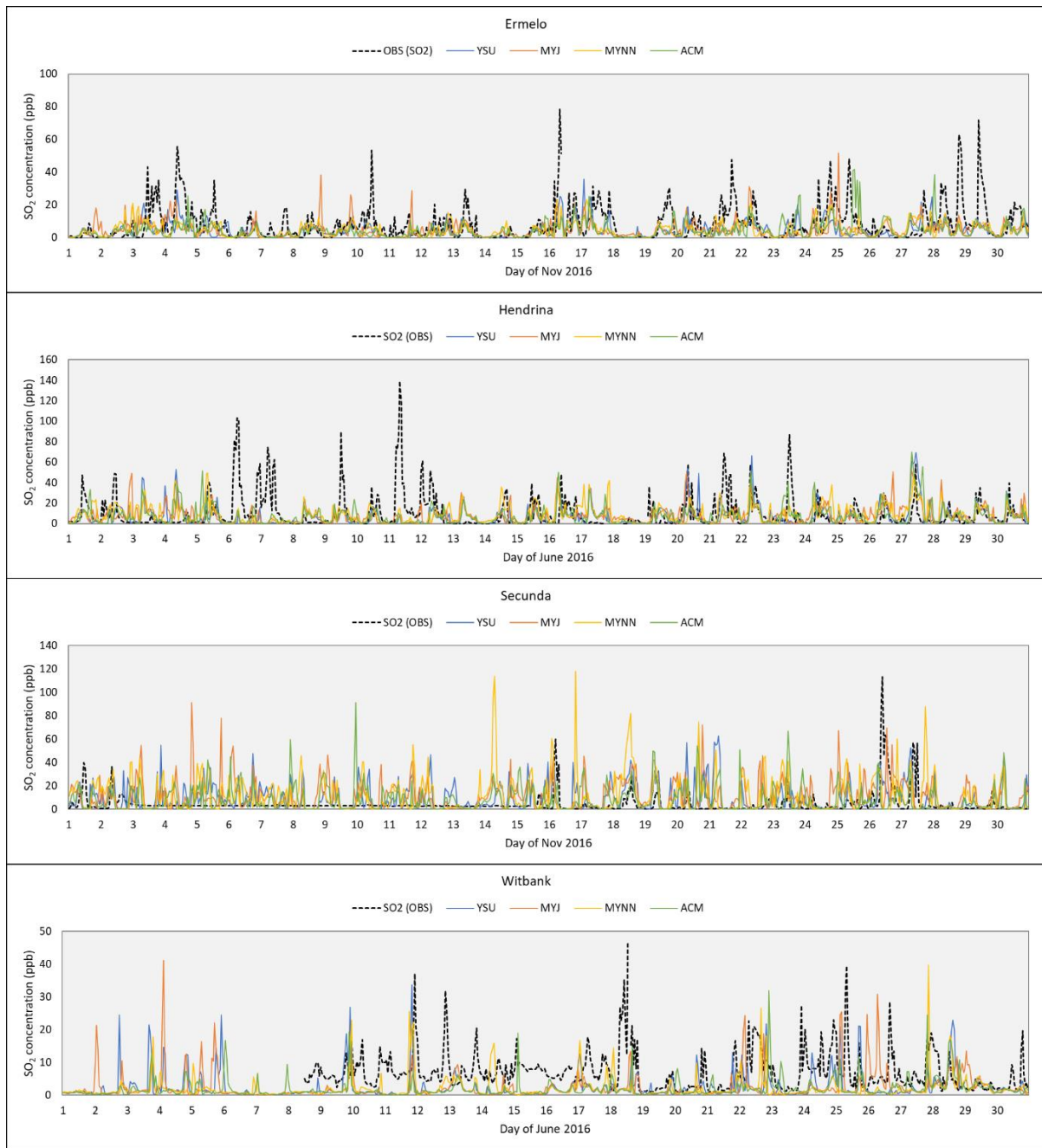


Figure B10. Hourly time series of observed and simulated SO₂ concentrations for November. An asterisk (*) indicates sites with anomalous data.

Appendix C: SO₂ spatial plots

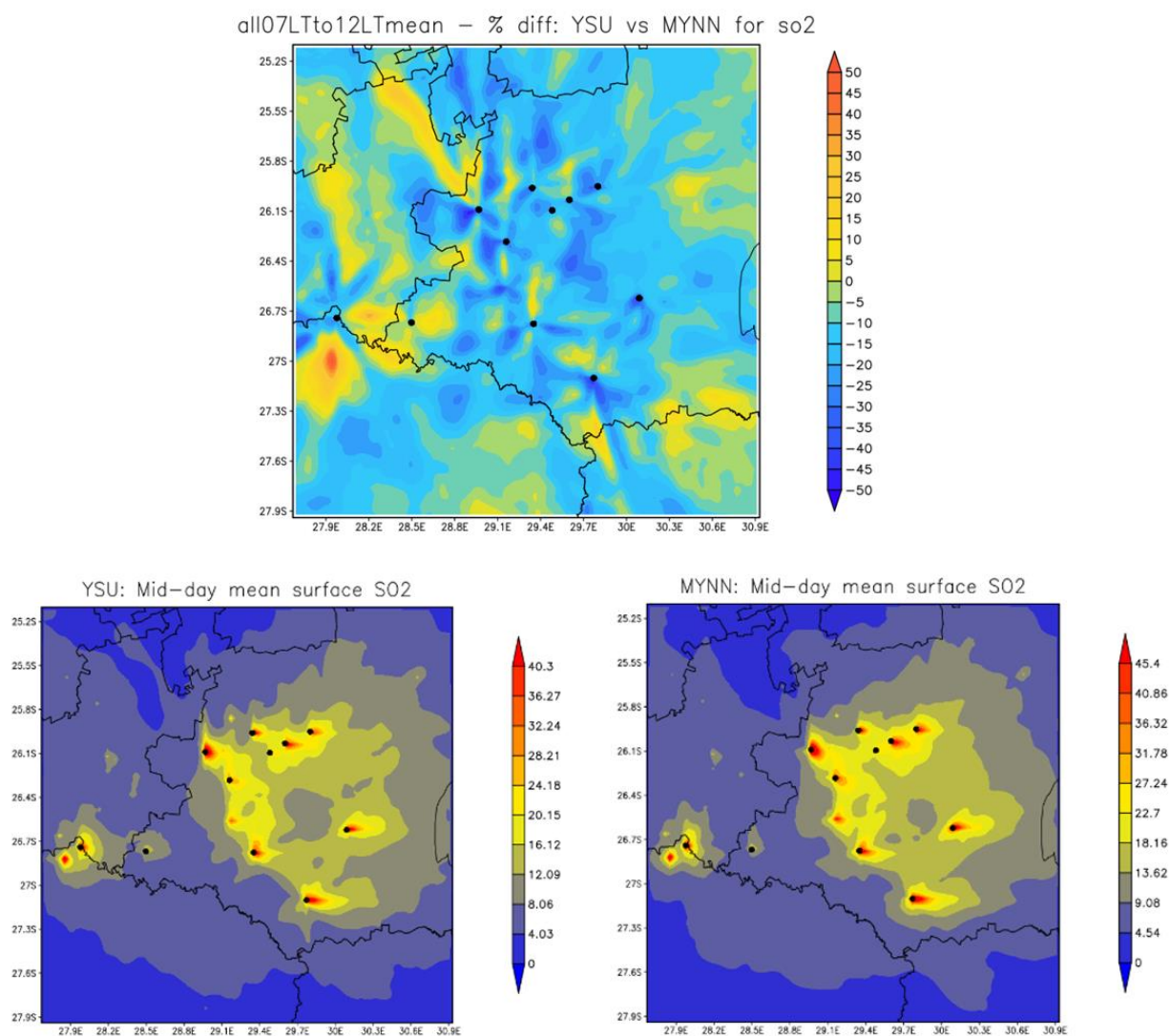


Figure C1. Average percentage (%) difference in simulated ground-level SO₂ concentration from 07 to 12 LT for YSU vs MYNN (top), and mean SO₂ concentrations for YSU (bottom left) and MYNN (bottom right) schemes during the same period. Note the different scales of the two bottom plots.

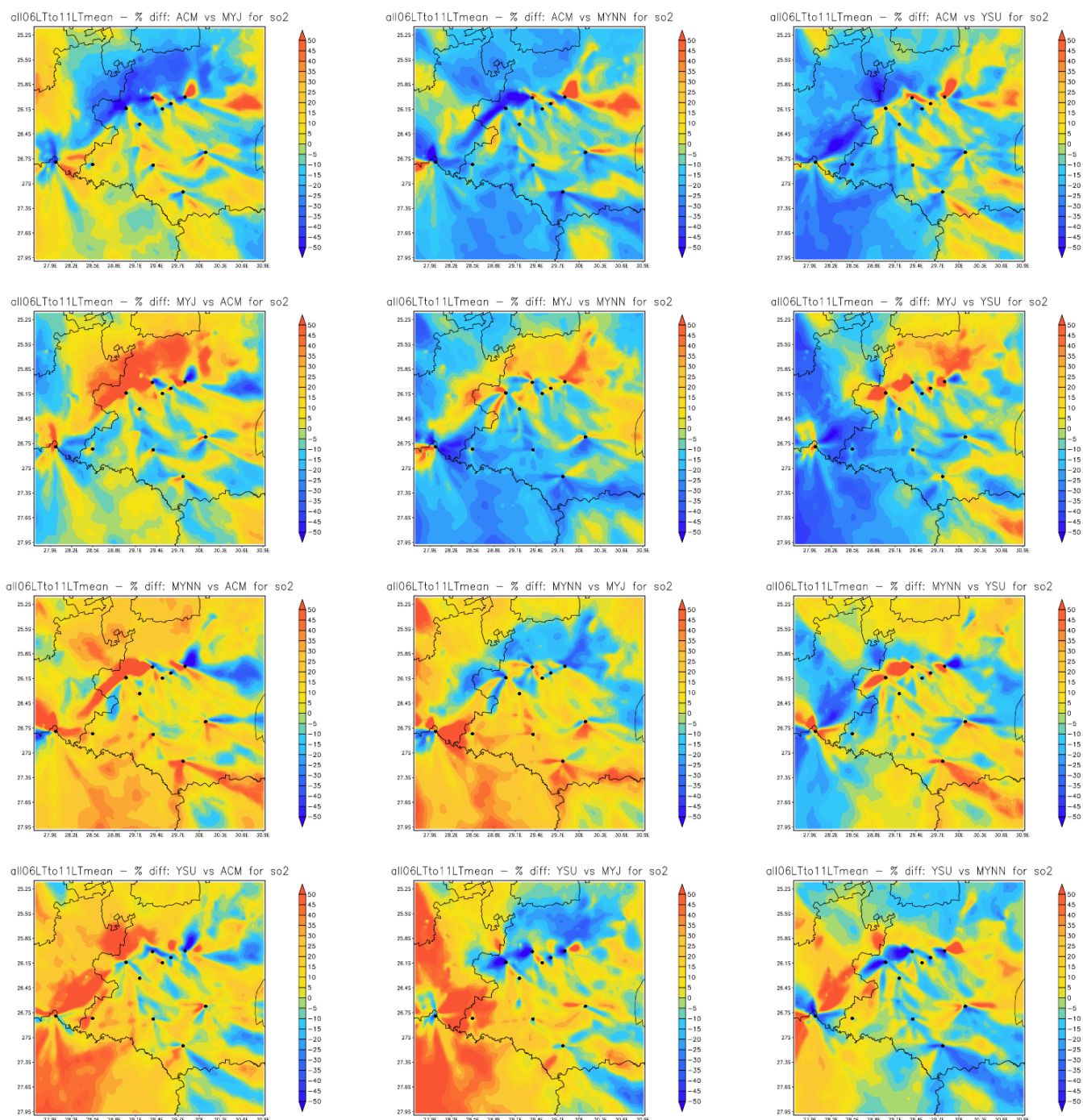


Figure C2. Average percentage (%) difference in simulated ground-level SO₂ concentration from 06 to 11 LT for different scheme combinations during November. Tall stacks from power generating facilities are indicated with black circles.